

1 Investigating small ion number size distributions: 2 insight into cluster formation and growth

3 Santeri Tuovinen¹, Janne Lampilahti¹, Nina Sarnela¹, Chengfeng Liu¹, Yongchun Liu² and Markku
4 Kulmala¹ and Veli-Matti Kerminen¹

5 ¹Institute for Atmospheric and Earth System Research/Physics, Faculty of Science, University of
6 Helsinki, Helsinki, Finland

7 ²Aerosol and Haze Laboratory, Beijing Advanced Innovation Center for Soft Matter Science and
8 Engineering, Beijing University of Chemical Technology, Beijing, China

9
10 **Correspondence:** Santeri Tuovinen (santeri.tuovinen@helsinki.fi) and Markku Kulmala
11 (markku.kulmala@helsinki.fi)

12 Abstract

13 Small ions, consisting mostly of charged molecular clusters with mobility diameters below 2 nm,
14 exist continuously in the atmosphere. Here, we studied small ion number size distributions
15 measured with Neutral cluster and Air Ion Spectrometer measurements in Hyytiälä, Finland and
16 Beijing, China. We found that in Hyytiälä, there is a strong positive relationship between the
17 concentration and diameter of small ions of both polarities and highly oxidized organic molecule
18 (HOM) and sulfuric acid concentrations, and that the relationship with the former is especially
19 strong. The relationship between the negative sulfuric acid cluster ions and the small ion number
20 size distribution in Hyytiälä was found to be more complex, but overall positive. In contrast to
21 Hyytiälä, we found that in Beijing the small ion number size distribution does not have a clear
22 relationship with sulfuric acid or oxidized organic molecule (OOM) concentration. We found that
23 the small ion size distribution in Hyytiälä behaved as expected with respect to varying coagulation
24 sink (CoagS), with concentrations of the smallest ions decreasing most with increasing CoagS.
25 Surprisingly, the small ion size distribution in Beijing did not vary significantly with varying
26 CoagS. However, in both locations, the impact of growth on the small ion number size distribution
27 during periods of intense cluster formation and new particle formation is clearly seen. Our results
28 show that while in Hyytiälä the growth of small ions to larger diameters is limited by the
29 concentrations of sulfuric acid and OOMs, in Beijing there are additional factors required for the
30 small ions to grow.

31 1 Introduction

32 Atmospheric aerosol particles influence the Earth's climate (e.g., Quaas et al., 2009; Boucher et al.,
33 2013; Schmale et al., 2021; Li et al., 2022) and can have adverse effects on human health (e.g.,
34 Shiraiwa et al., 2017; Arfin et al., 2023). These influences have commonly been related to
35 properties, such as the mass or number concentration of an atmospheric aerosol population, its size
36 distribution, or its chemical composition (Shiraiwa et al., 2017; Atkinson et al., 2015; Finlay, 2021).
37 The electric charge state of atmospheric aerosols has attracted much less interest, although this
38 property may have large influences on the dynamics of atmospheric aerosol populations (Harrison
39 and Carslaw, 2003; Fdez-Arroyabe et al., 2022), thereby affecting many other important aerosol

40 properties. The presence of charges also makes it possible to measure low aerosol concentrations at
41 high resolution in both time and particle size (Mirme and Mirme, 2013; Mirme et al., 2024).

42 Charged atmospheric particles, or more broadly ions, include charged aerosol particles, charged
43 molecular clusters, and even large molecules having a charge. Ions with electrical mobility
44 diameters roughly below 2 nm in diameter are classified as small ions, and consist of charged
45 molecular clusters, while ions above 2 nm consist of charged aerosol particles (Tammet, 1995; Ehn
46 et al., 2010). Of these charged aerosol particles, those with diameters between 2 and 7 nm are
47 referred to as intermediate ions (Tammet, 1995).

48 Atmospheric ions are created through ionization of molecules the atmosphere. Most important of
49 these ionization sources are cosmic ray radiation, gamma radiation, and radon decay (Harrison and
50 Tammet, 2008). Small ions are constantly present in the troposphere as molecules are ionized and
51 subsequently grow to small ions (Harrison and Tammet, 2008; Hirsikko et al., 2011). The lifetime of
52 small ions is short at around 100 s, and their chemical composition depends on the atmospheric
53 trace gas concentrations and their chemistry (Harrison and Tammet, 2008; Ehn et al., 2010; Shuman
54 et al., 2015). In contrast, intermediate ions are typically detected mainly during the occurrence of
55 atmospheric new particle formation (Tammet et al., 2014, Tuovinen et al., 2024), or during snowfall
56 or rain (Hirsikko et al., 2007; Tammet et al., 2014). New particle formation (NPF) is considered to
57 occur when constantly existing stable clusters, neutral or charged, start to grow to larger sizes by
58 uptake of precursor vapors such as sulfuric acid and organic compounds with low volatilities
59 (Kulmala et al., 2006; Kulmala et al., 2007; Lehtipalo et al., 2018; Kirkby et al., 2023).

60 A recent study by Kulmala et al. (2024a) presented the use of a novel cluster ion counter (CIC) for
61 measuring small and intermediate ion concentrations to study local-scale NPF and to derive other
62 parameters such as condensation sink (CS). The information gained by these measurements can be
63 used further to study the complex climate-biosphere feedbacks (Kulmala et al., 2020; Kulmala et
64 al., 2024b). These recent advances have motivated us to take a deeper look at the small ion size
65 distribution.

66 The concentration of small ions depends on the ionization rate and the loss rate of small ions due to
67 ion-ion recombination, coagulation with larger aerosol particles, and deposition (Tammet et al.,
68 2006; Hörrak et al., 2008). The size of the small ions depends on their chemical composition and
69 age as the ions grow through chemical reactions and condensation of vapors, or through coagulation
70 with neutral clusters. We can learn more about these chemical and dynamical processes by
71 investigating the small ion number size distributions.

72 In this study, we combine ion number size distribution data measured by Neutral cluster and Air Ion
73 Spectrometer (NAIS; Manninen et al., 2009; Mirme and Mirme, 2013) with concentrations of low-
74 volatility vapors and ion clusters measured by mass spectrometer instruments to identify how, and
75 why, the size distribution of small ions changes and evolves. Data from two different contrasting
76 locations, Hyytiälä, Finland and Beijing, China (Kulmala et al., 2025), are used. First, we will study
77 if the variation of the small ion size distribution with season is considerable. Secondly, we will
78 quantify the potential relationship of organic low-volatility vapors and sulfuric acid on the size and
79 number of small ions. Third, we will analyze the impact of coagulation scavenging on small ion size
80 distribution. Fourth, we will analyze the small ion size distribution as a function of intensity of NPF
81 to reveal how the small ion size distribution changes as the clusters grow. Finally, some case studies

82 are presented. With these, we aim to identify the most important processes impacting the small ion
 83 number size distribution, and to evaluate the role of these processes in driving the growth of small
 84 ions to intermediate ions.

85 **2 Background and methods**

86 **2.1 Evolution of small ion size distribution**

87 Typically, the parameter of interest when small ions are considered is their total number
 88 concentration and its temporal evolution. The changes in the small ion number concentration can be
 89 described by the simplified air ion balance equation:

$$\frac{dN^{\pm}}{dt} = Q - CoagS N^{\pm} - \alpha N^{\pm} N^{\mp} - S N^{\pm} \quad (1)$$

90 Here, N^{\pm} is the concentration of one polarity, while N^{\mp} is the concentration of the other polarity.
 91 The first term on the right-hand side of the equation describes the source rate of the ions, where Q is
 92 the ionization rate of air molecules. The second term, where CoagS stands for coagulation sink,
 93 tells the loss rate of small ions due to coagulation on larger aerosol particles. The third term tells the
 94 loss rate of ions due to ion-ion recombination, where α is the ion recombination coefficient. The
 95 final term describes other losses of the ions, including deposition, and S is the loss rate of the ions to
 96 these other sinks.

97
 98 As we can see, the above equation does not explicitly depend on the size of the small ions nor can it
 99 be directly used to describe the evolution of the size-dependent small ion size distribution. The time
 100 evolution of small ions of certain size i are described by the charged general dynamics equations
 101 (charged GDEs; Kulmala et al., 2012):

$$\frac{dN_i^{\pm}}{dt} = J_i + \chi N_i N_{d<i}^{\pm} - N_i^{\pm} CoagS_i - \alpha N_i^{\pm} N_{d<i}^{\mp} - \frac{GR}{\Delta d_i} N_i^{\pm} \quad (2)$$

102 Here, J_i is the formation rates of ions of size i . The second term on the right-hand side represents the
 103 charging of neutral clusters by ions smaller than i , where χ is the ion-cluster attachment coefficient.
 104 The last term, where GR is the ion growth rate, describes the growth of ions i to larger sizes.
 105 Considering Eq. 2, we can see that an increasing GR will shift the ion size distribution towards
 106 larger diameters. CoagS is the highest for the smallest ions and if it increases, the concentrations of
 107 smallest ions are decreasing the most, causing an apparent shift in the distribution towards larger
 108 diameters. However, CoagS also affect the lifetime of small ions, so that with an increasing CoagS
 109 the ions have less time to grow, reducing the concentration of larger small ions. If ion
 110 concentrations are high, ion-ion recombination rate will be higher, which will also lead to shorter
 111 small ion lifetime and possibly smaller concentrations of larger small ions. Through ion-cluster
 112 attachment, the small ion size distribution depends on the size distribution of neutral clusters,
 113 although this term is relatively small when compared to the coagulation loss and growth terms.

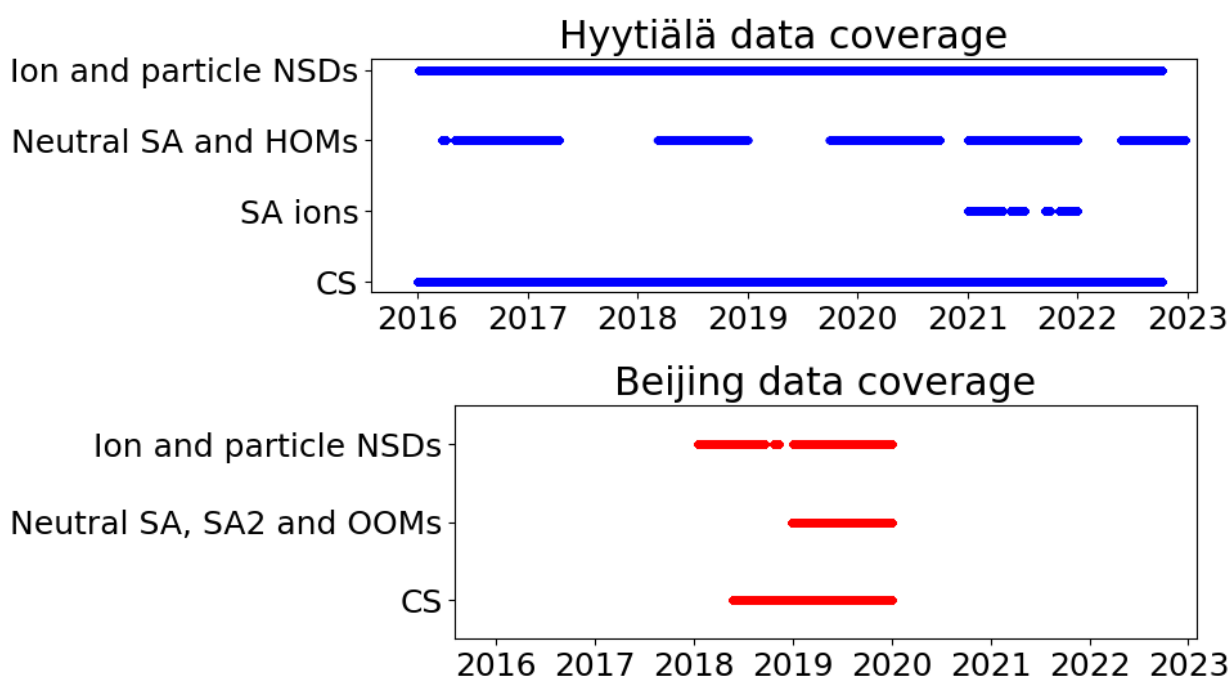
114 We assume that the role of direct transport of clusters on the changes in the small ion size
 115 distribution is negligible due to their short lifetime of just a couple of minutes (Tamm et al.,
 116 2006). Therefore, the observations are assumed to be very local. However, transport can indirectly
 117 impact the size distribution of small ions i.e., through transport of trace gases and larger particles.
 118 We also note that while meteorological conditions, such as temperature, strongly influence

119 processes such as HOM formation (e.g., Quéléver et al., 2019), we do not explicitly consider them
120 in this study.

121 2.2 Measurement sites

122 Two different locations were considered in this study: SMEAR II measurement station in Hyytiälä,
123 Finland (61°51' N, 24°17' E) and BUCT/AHL measurement station in Beijing, China (39°94' N,
124 116°30' E). The former is a rural site surrounded by boreal forest while the latter is an urban site
125 close to residential building and traffic roads. For more details on SMEAR II station, see Hari and
126 Kulmala. (2005). For more details on BUCT/AHL site, see Liu et al. (2020). These two locations
127 are included in the analysis due to their contrasting natures, providing an opportunity for insight
128 into the variation of small ion size distribution and small ion dynamics in different environments.

129 2.3 Measurement and other data



130 **Fig.1:** Data coverage for the two sites, Hyytiälä, Finland, and Beijing, China, from which data were
131 used in this study. NSD refers to number size distribution, while SA refers to sulfuric acid, SA2 to
132 neutral sulfuric acid dimer, HOM to highly oxidized organic molecule and OOM to oxidized
133 organic molecule. CS refers to condensation sink.

134
135
136 Atmospheric ion and total particle number size distributions in Hyytiälä and Beijing were measured
137 with Neutral cluster and Air Ion Spectrometer (NAIS; Manninen et al., 2009; Mirme and Mirme,
138 2013). The NAIS measures both charged and total particle number size distributions in the ranges
139 0.8-42 nm and 2.5-42 nm, respectively. Main focus of the analysis in this study is on the number
140 size distributions of small ions (diameters below 2.0 nm). Ion concentrations between 2.0 and 2.3
141 nm were used to characterize the intensity of local clustering (Tuovinen et al., 2023) and new
142 particle formation ranking data, characterizing the intensity of NPF, were also used. The NPF
143 ranking was based on the total particle number concentration between 2.5 and 5.0 nm and
144 determined according to the method presented by Aliaga et al. (2023).

145 The chemical composition of small ions typically differs between the polarities (Ehn et al., 2010;
146 Zha et al., 2023). For example, Ehn et al. (2010) found that in Hyttiälä the daytime negative small
147 ions consisted largely of sulfuric acid clusters, while positive small ions consisted of organic species
148 such as alkyl pyridines and alkyl amines. Therefore, we cannot assume that the negative and
149 positive small ion populations behave similarly with respect to i.e., increased sulfuric acid
150 concentrations. Thus, both negative and positive polarity were separately considered.

151 All diameters used in study are electrical mobility diameters. We note that especially for the
152 smallest of the ions the mobility diameter may not accurately describe the physical dimensions of
153 the ion (see e.g., Ehn et al., 2011). Regardless, we refer to diameter rather than the electrical
154 mobility as we see it as a more intuitively understandable parameter for the ion size.

155 From Hyttiälä, concentrations of neutral sulfuric acid and highly oxidized organic molecules
156 (HOMs) were used to study the influence of cluster formation and growth on the small ion size
157 distribution. These were measured with Chemical Ionization Atmospheric Pressure interface Time-
158 Of-Flight (CI-APi-TOF) mass spectrometer (Jokinen et al., 2012). In addition, the signal counts of
159 ionized sulfuric acid clusters measured with APi-TOF were used to give further insight into the
160 composition of the small ions. The signal counts in the study are given as relative signals to the total
161 measured ion current. From Beijing, neutral sulfuric acid, sulfuric acid dimer and total oxidized
162 organic molecule (OOM) concentrations, which were measured with a nitrate based – long time-of-
163 flight chemical ionization mass spectrometer (CIMS), were included in the analysis. We note that
164 we use the term OOM instead of HOM for the organic molecules in Beijing based on previous
165 results by Yan et al. (2021), suggesting that most of these measured organic molecules in Beijing do
166 not meet the requirements for HOMs (see Bianchi et al., 2019).

167
168 Condensation sinks (CS) for both sites were included in the analysis as proxies for the coagulation
169 scavenging of the small ions. In Hyttiälä, the particle size distributions from which CS was derived
170 from were measured with a twin Differential Mobility Particle Sizer (DMPS) system (Aalto et al.,
171 2001). In Beijing, the particle size distributions for CS were measured with a particle size
172 distribution (PSD) system (Liu et al., 2016).

173
174 Data coverage for both sites is presented in Fig. 1.

175 **2.4 Determining the average small ion diameter**

176 From the small ion number size distributions, we determined the mean mobility diameter (d_{mean}),
177 and median mobility diameter (d_{median}) of small ions. First, cubic interpolation was applied to the
178 measured ion number size distributions. We note that nearest neighbor and linear interpolation
179 methods were also tested, and the influence of the chosen method on the value of d_{mean} or d_{median} was
180 found minor. The diameter range for the interpolation was from the lower detection limit to 2.0 nm
181 with a step of 0.001 nm. Then, d_{peak} was determined by finding the diameter corresponding to the
182 maximum concentration of small ions. Weighted mean and median were used to determine d_{mean} and
183 d_{median} , with the number concentrations of ions below 2 nm in diameter used as weights. The
184 equation below was used to find weighted mean diameter:

$$185 \quad d_{mean} = \frac{\sum N_i d_i}{\sum N_i}, \quad (3)$$

186 where d_i is the diameter of ions of a certain size and N_i is their number concentration. The weighted
187 median was determined by finding the diameter d_j satisfying

$$j = \min_k \left[\sum N_i d_i > \frac{1}{2} \sum N_i d_i \right]. \quad (4)$$

188

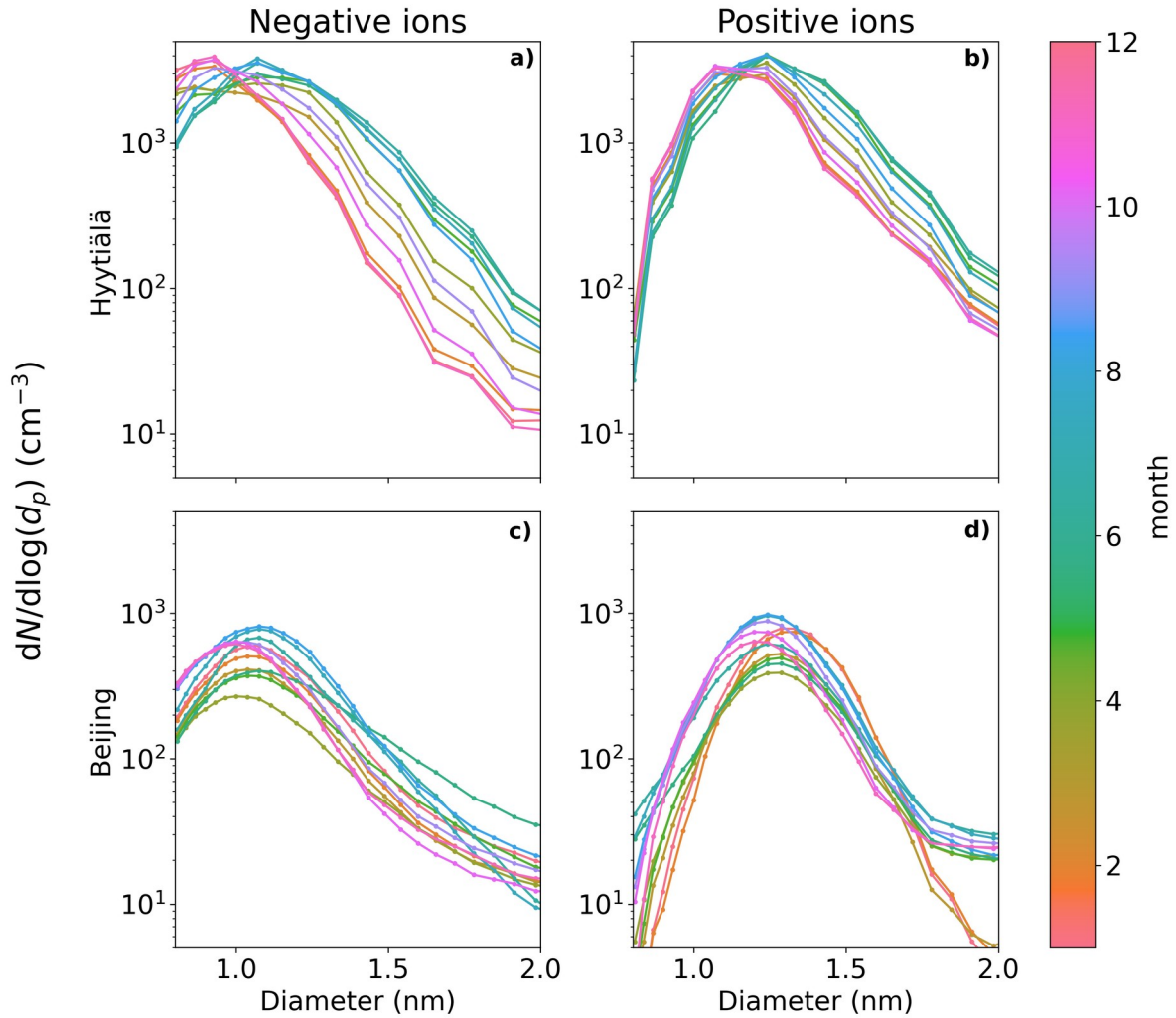
189 **3 Results**

190 **3.1 Seasonal variation of the small ion size distribution**

191 The Fig. 2a and b show the monthly median negative and positive ion distributions between 0.8 and
192 2.0 nm in Hyytiälä. Table 1 records the monthly mean and median diameters (d_{mean} and d_{median}). Clear
193 month-to-month changes in the size distributions are observed, and these are more pronounced for
194 negative ions (Fig. 2a). During winter, the concentration of negative ions peaks already below 1.0
195 nm, while during summer the highest concentration is observed between 1.1 and 1.2 nm. In
196 addition, the concentrations of negative ions above 1.1 nm are increased from winter to summer.
197 Close to 2.0 nm the ion concentration is almost one order of magnitude higher during summer. This
198 behavior of the size distribution is reflected in the values of d_{mean} and d_{median} , which are smallest
199 during December and January, with $d_{\text{mean}} = 0.99$ nm and $d_{\text{median}} = 0.95$ nm, and the largest during
200 June and July, with $d_{\text{mean}} = 1.15$ nm and $d_{\text{median}} = 1.11$ nm.

201 Positive ion size distributions (Fig. 2b) behave similarly to the negative ones, however the changes
202 are less pronounced. Above 1.4 nm and up to 2.0 nm, the concentrations are roughly twice as high,
203 or less, during summer compared to winter. For positive small ions, the smallest value of $d_{\text{mean}} =$
204 1.16 and $d_{\text{median}} = 1.13$ nm (December and January) and the largest value of $d_{\text{mean}} = 1.29$ nm and
205 $d_{\text{median}} = 1.27$ nm (June). The difference between the average diameters of negative and positive
206 small ions was around 0.15 nm, in line with previous studies (e.g., Hörrak et al., 2000).

207 The observed seasonal behavior of the size distributions in Hyytiälä follow expectations: during
208 spring and summer, the concentrations of low-volatility vapors are much higher due to increased
209 solar radiation and organic emissions (Sulo et al., 2021). Therefore, small ions should be able to
210 grow to larger diameters due to the uptake of these vapors. We will look further into how the small
211 ion size distribution varies with respect to low volatile vapor concentrations in Sect. 3.2.



212
 213 **Fig. 2:** Median monthly sub-2 nm negative (a, c) and positive (b, d) ion size distributions for
 214 Hyytiälä (a, b) and Beijing (c, d). The different months are marked by the different colors.
 215

216 The Fig. 2c, d show the monthly median negative (Fig. 2c) and positive (Fig. 2d) ion distributions
 217 between 0.8 and 2.0 nm in Beijing, while Table 2 records the monthly d_{mean} and d_{median} . As expected
 218 due to the high CoagS (Eq. 1,2, and Fig. A1), the concentrations are lower than in Hyytiälä. For
 219 negative ions (Fig. 2c), the concentrations during summer are higher than in other seasons below
 220 1.6 nm and lower than in other seasons close to 2.0 nm. During spring, the concentrations of
 221 negative ions below 1.4 nm are lower than in other seasons. The smallest value of negative d_{mean}
 222 and d_{median} are in November, $d_{\text{mean}} = 1.04$ nm and $d_{\text{median}} = 1.01$ nm. The largest values are during June,
 223 $d_{\text{mean}} = 1.16$ nm and $d_{\text{median}} = 1.12$ nm.

224 For positive small ions in Beijing (Fig. 2d), the concentrations of both the smallest and the largest
 225 ions in the 0.8 to 2.0 nm range are both considerably lower from January to March compared to the
 226 later months. Otherwise, it is hard to identify a clear seasonal pattern. The largest positive average
 227 diameter is during February, $d_{\text{mean}} = 1.32$ nm and $d_{\text{median}} = 1.31$ nm, while the smallest values are in
 228 November, $d_{\text{mean}} = 1.22$ nm and $d_{\text{median}} = 1.21$ nm.

229 Compared to Hyytiälä, the seasonal trends in Beijing are not as clear or strong, which implies that
 230 the factors controlling the small ion size distribution are less seasonal in Beijing than in Hyytiälä,

231 where the small ion size distribution show a strong seasonal variation. However, we note that
 232 because there are less data from Beijing compared to Hyytiälä, variation between years can have a
 233 larger impact on the results than in Hyytiälä.

234

235 **Table 1:** Mean and median monthly diameters (nm) of ions between 0.8 and 2.0 nm in Hyytiälä.

236 *The highest concentration corresponds to the lowest detected diameter.

Month	Negative ions		Positive ions	
	d_{mean}	d_{median}	d_{mean}	d_{median}
1	0.99	0.95	1.16	1.13
2	1.00	0.96	1.17	1.15
3	1.05	1.02	1.2	1.18
4	1.08	1.06	1.21	1.20
5	1.12	1.10	1.27	1.25
6	1.15	1.11	1.29	1.27
7	1.15	1.11	1.28	1.26
8	1.13	1.10	1.25	1.23
9	1.11	1.08	1.22	1.20
10	1.05	1.02	1.19	1.17
11	1.01	0.98	1.17	1.14
12	0.99	0.95	1.16	1.13

237

238

239 **Table 2:** Mean and median monthly diameters (nm) of ions between 0.8 and 2.0 nm in Beijing.

240 *The highest concentration corresponds to the lowest detected diameter.

Month	Negative ions		Positive ions	
	d_{mean}	d_{median}	d_{mean}	d_{median}
1	1.10	1.07	1.30	1.30
2	1.09	1.06	1.32	1.31
3	1.09	1.06	1.28	1.27
4	1.10	1.05	1.28	1.26
5	1.12	1.07	1.28	1.27
6	1.16	1.12	1.27	1.26
7	1.12	1.08	1.25	1.24
8	1.10	1.08	1.25	1.24
9	1.10	1.07	1.25	1.24
10	1.07	1.03	1.24	1.23

11	1.04	1.01	1.22	1.21
12	1.05	1.01	1.23	1.21

241

242

243 **3.2 Potential impact of low volatility vapors to small ion size distribution** 244 **in Hyytiälä**

245 **3.2.1 Highly oxidized organic molecules (HOMs)**

246 Fig. 3 shows the median ion number size distributions between 0.8 and 2.0 nm in Hyytiälä with
247 respect to varying neutral highly oxidized organic molecule (HOM) concentration. HOM
248 monomers, HOM dimers and total HOM are considered separately. Results for daytime (10:00-
249 16:00) and evening (18:00-00:00) are both presented (Fig. 3a and 3b, respectively). The HOM
250 concentrations are divided into percentiles.

251 A clear increase in the number of negative ions (Fig. 3a, i-iii, Fig. 3b, i-iii) above approx. 1.05 nm,
252 and for positive ions (Fig. 3a, iv-vi, Fig. 3b, iv-vi) slightly larger than that, is seen with an
253 increasing HOM concentration for all three HOM categories. The differences are the largest for
254 HOM monomers (i, iv) and HOM total (iii, vi), which is mainly dominated by the HOM monomers.
255 The differences are also stronger for negative ions than positive ions, and are stronger during the
256 evening (Fig. 3b) compared to daytime (Fig. 3a).

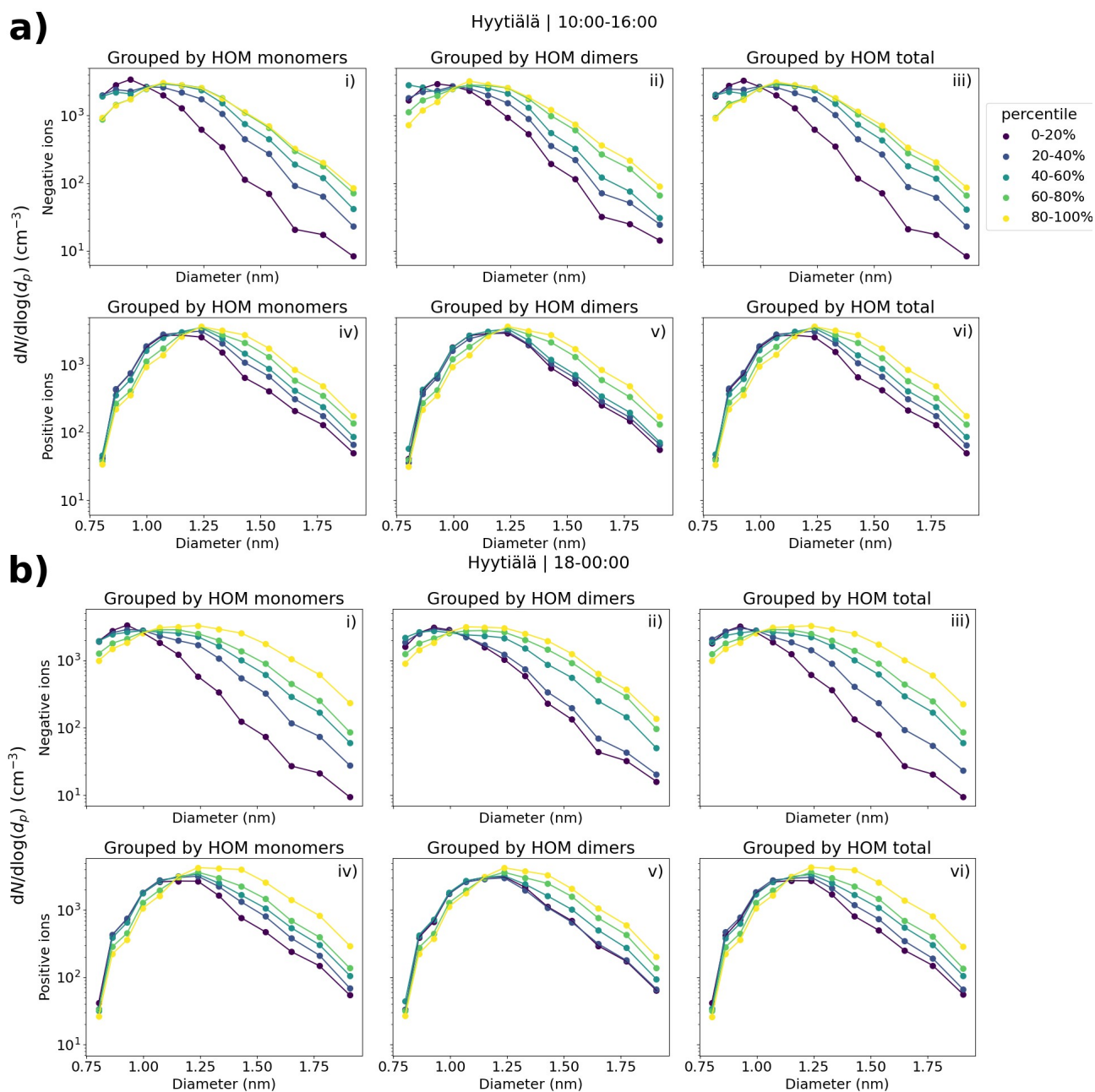
257 Comparing the negative ion size distributions between the HOM percentiles of 0-20% and 80-
258 100%, we see that the difference in the concentrations increases with an increasing diameter, and
259 that close to 2.0 nm this difference is approximately one order of magnitude during daytime (Fig.
260 3a,i-iii) and a bit more during the evening (Fig. 3b, i-iii). Comparing the similar negative ion
261 concentrations when HOM monomer concentration during the evening is in the 80-100% percentile
262 compared to 0-20%, there's approx. a 0.5 nm shift in the diameters (Fig. 3b, i), which is a big
263 difference for the sub-2 nm ion population.

264 In line with the large differences in the small ion size distributions in Fig. 3 with respect to HOM
265 concentration, a strong correlation between the small ion d_{mean} and the HOM concentrations was
266 seen (Fig. 4). The Spearman correlation coefficients (r_s) between d_{mean} and HOMs were 0.6 or
267 above, for both daytime and evening. For daytime, the best correlation was between d_{mean} of positive
268 ions and HOM monomer concentration, $r_s = 0.74$ (Fig. 4e). During nighttime, the strongest
269 correlation was between d_{mean} of negative ions and HOM monomer concentration, $r_s = 0.73$ (Fig.
270 4c).

271 The clear correlation between HOMs and the small ion size distribution in Hyytiälä suggests a
272 strong impact of organic compounds to the small ion population. This interpretation, as opposed to
273 the correlation being due to a correlation with another variable such sulfuric acid concentration, is
274 supported by the observation of the correlation being stronger during evening when the
275 concentrations of other precursors such as sulfuric acid are lower and organic ion cluster formation
276 is known to take place in Hyytiälä (Mazon et al., 2016; Rose et al., 2018). We note that part of the
277 increase in the diameters of the small ions when HOMs are abundant could be due to the large size
278 of organic molecules when compared to sulfuric acid molecules. However, the clear increase in

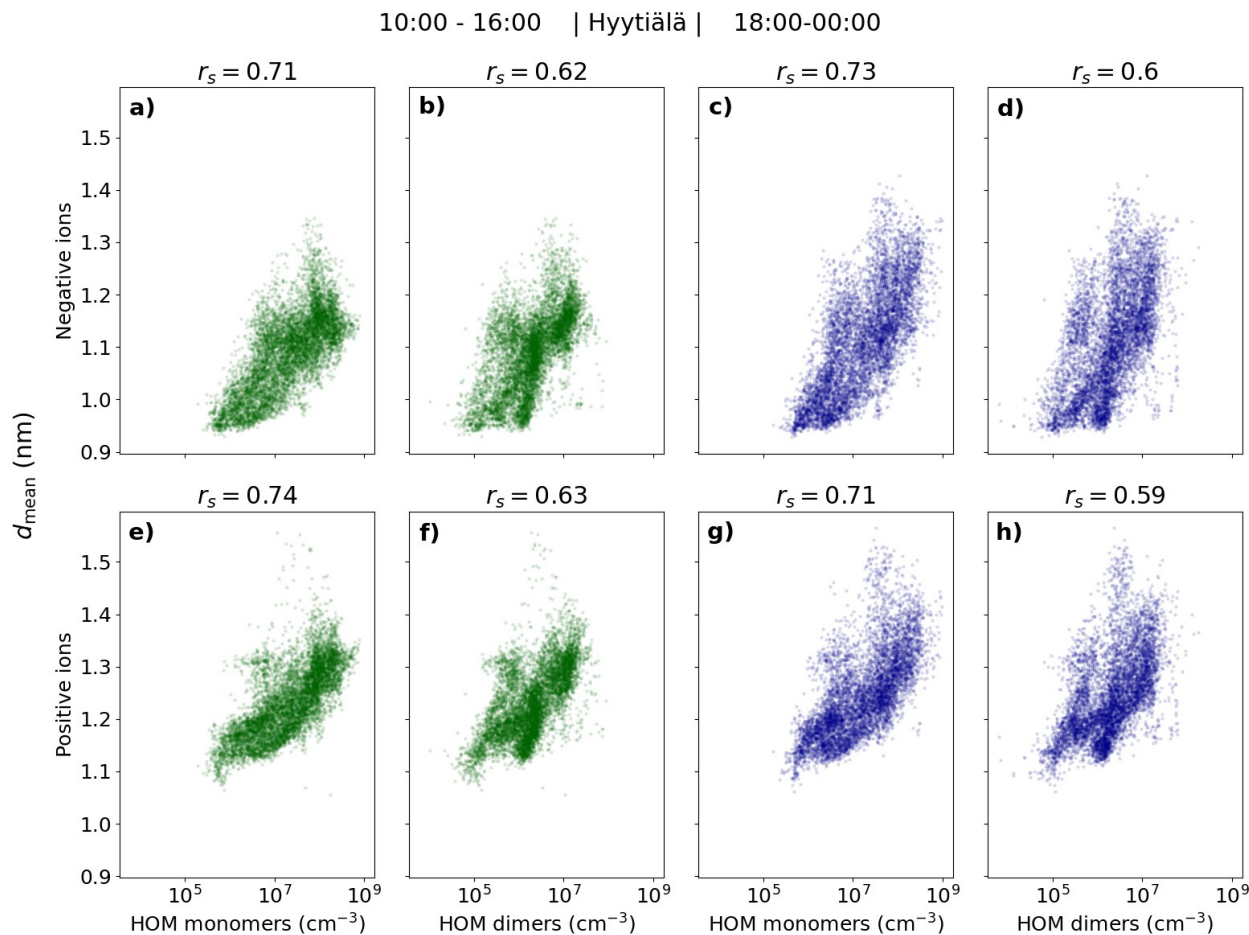
279 concentrations even close to 2.0 nm suggests that the impact is mainly due to the growth of small
 280 ions by the uptake of organic vapors.

281 While the concentrations of larger small ions of both polarities increase with increasing HOM
 282 percentile, the differences are larger for the negative ions (Fig. 3). This could be due to the uptake
 283 of organics being more effective for the negatively charged ions. However, the equally strong
 284 correlation between d_{mean} of positive small ions and HOM concentrations does not support this
 285 interpretation. A possible explanation is the size difference between the negative and positive small
 286 ions: due to the larger diameter of positive small ions, it might be that the impact of the growth to
 287 the diameters of the positive ions is not as large. For a larger cluster (ion), more molecules are
 288 needed to increase the diameter equally than for a smaller one.



289
 290 **Fig. 3:** The median negative (i-iii) and positive (iv-vi) small ion (sub-2 nm) size distributions in
 291 Hyytiälä, Finland grouped by the percentiles of neutral HOM monomer (i, iv), HOM dimer (ii, v)
 292 and total HOM (iii, vi) concentrations. Both the evening (18:00-00:00) size distributions (b) and

293 daytime (10:00-16:00) size distributions (a) are shown. Daytime percentiles for HOM monomers,
 294 dimers and total are 20%: $4.30 \cdot 10^6$, $5.93 \cdot 10^5$, and $5.10 \cdot 10^6$ cm^{-3} ; 40%: $1.34 \cdot 10^7$, $1.45 \cdot 10^6$, and
 295 $1.50 \cdot 10^7$ cm^{-3} ; 60%: $4.00 \cdot 10^7$, $2.44 \cdot 10^6$, and $4.18 \cdot 10^7$ cm^{-3} ; 80%: $9.70 \cdot 10^7$, $7.62 \cdot 10^6$, and $1.05 \cdot 10^8$ cm^{-3} ,
 296 respectively. Evening percentiles for HOM monomers, dimers and total are 20%: $3.00 \cdot 10^6$,
 297 $4.94 \cdot 10^5$, and $3.75 \cdot 10^6$ cm^{-3} ; 40%: $8.40 \cdot 10^6$, $1.50 \cdot 10^6$, and $1.03 \cdot 10^7$ cm^{-3} ; 60%: $3.17 \cdot 10^7$, $2.95 \cdot 10^6$,
 298 and $3.65 \cdot 10^7$ cm^{-3} ; 80%: $7.52 \cdot 10^7$, $7.70 \cdot 10^6$, and $8.46 \cdot 10^7$ cm^{-3} , respectively.
 299



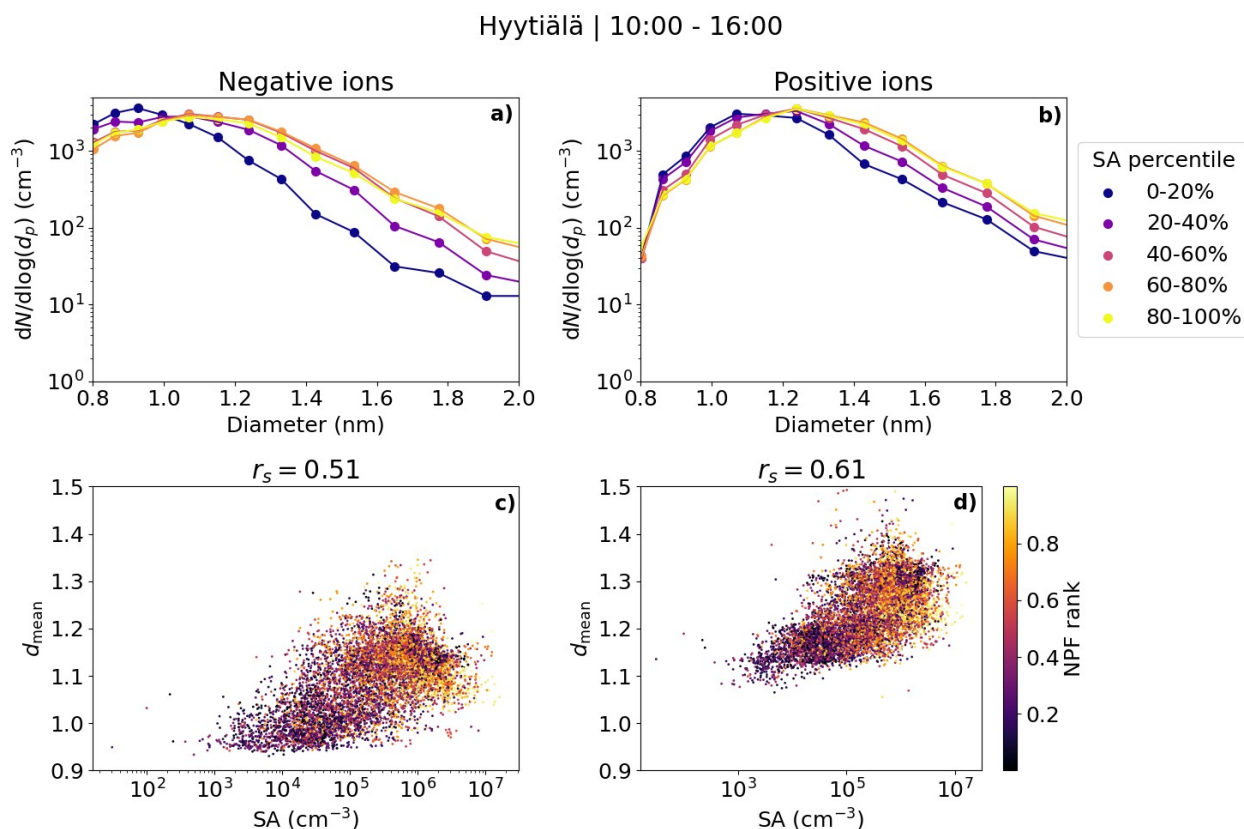
300
 301 **Fig. 4:** Mean diameter (d_{mean}) of negative (a-d) and positive (e-h) small (sub-2 nm) ions as a
 302 function of HOM (monomer, dimer and total) concentration in Hyytiälä. The individual points are
 303 hourly medians, and the daytime (10:00-16:00, marked in green) and evening (18:00-00:00, marked
 304 in dark blue) are shown separately. Spearman correlation coefficients (r_s) are shown.
 305

306 3.2.2 Sulfuric acid

307 Fig. 5 shows the median daytime negative and positive small ion (0.8-2.0 nm) size distributions
 308 grouped by the percentiles of neutral sulfuric acid (SA) concentration (Fig. 5a and b). In addition,
 309 the daytime hourly median d_{mean} values are shown as a function of the SA concentration (Fig. 5c and
 310 d). We see a clear increase in the concentrations of negative (positive) small ions larger than
 311 approximately 1.05 (1.1) nm when comparing SA concentrations in the lower percentiles to the
 312 higher percentiles, until the behavior seems to stall so that the 60-80% and 80-100% percentiles
 313 show similar size distributions. From previous studies, we know that while sulfuric acid is often
 314 needed for the initial cluster formation, organic compounds tend to drive the cluster growth (e.g.,

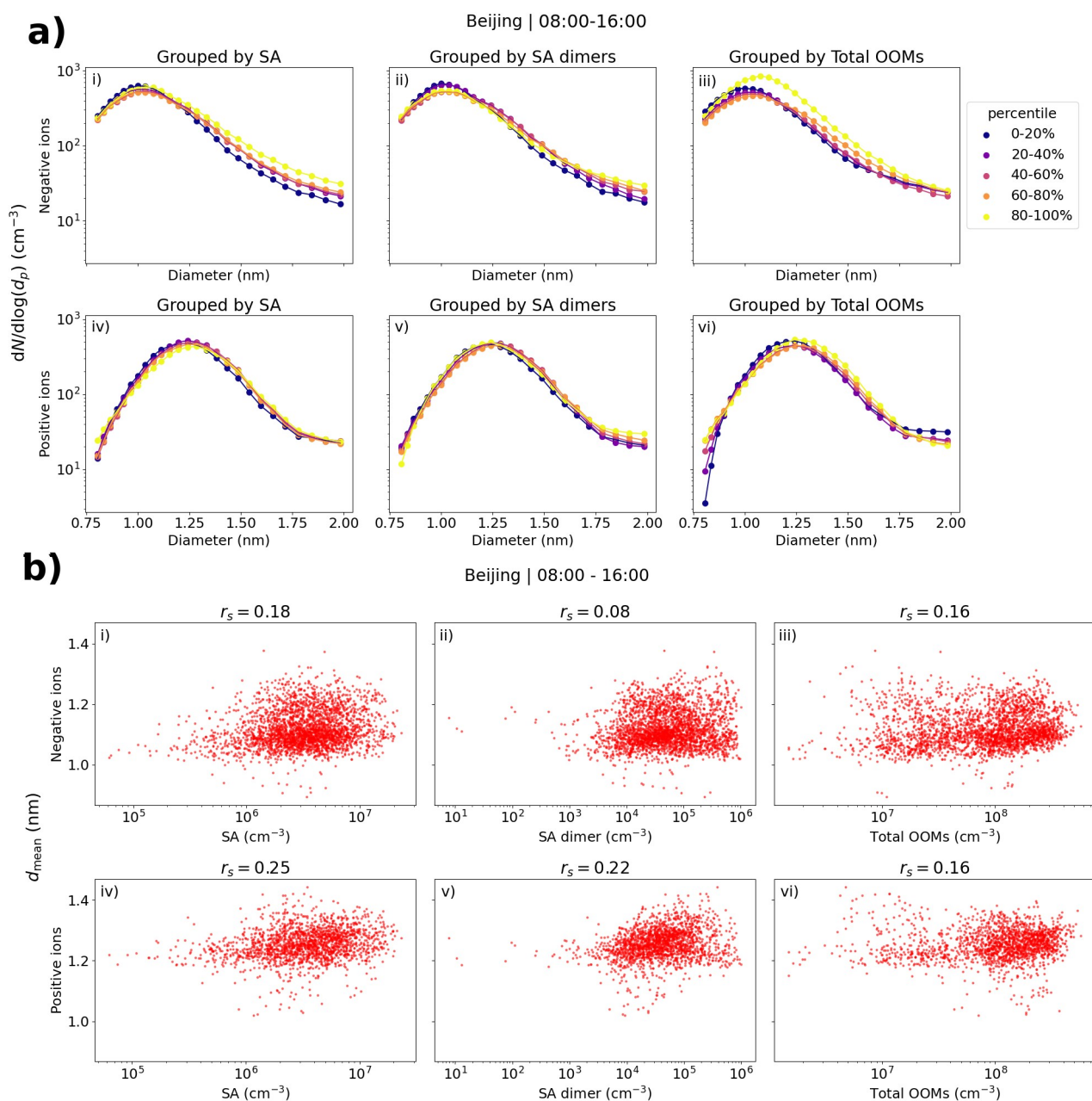
315 Kulmala et al., 2013). This could explain the lack of differences in the size distributions between the
 316 60-80% and 80-100% percentiles of the SA concentration.

317 A good positive correlation was seen between d_{mean} and SA concentration for both polarities, $r_s =$
 318 0.51 (0.61) for negative (positive) ions (Fig. 5c and d). The correlation is slightly weaker than what
 319 was observed between d_{mean} and HOM concentrations. The majority of d_{mean} values above 1.1 nm
 320 correspond to days with a high NPF ranking, while most values of d_{mean} below 1.1 nm correspond to
 321 days with low NPF rank values below 0.5. Notably, for d_{mean} of negative small ions above approx.
 322 1.1 nm, the values of d_{mean} do not seem to increase with an increasing SA concentration as clearly as
 323 they do with an increasing HOM concentration (Fig. 4). As discussed above, organic compounds
 324 might be needed to drive the growth of small ions further, and thus dependency of d_{mean} on SA is not
 325 seen as clearly when d_{mean} is above 1.1 nm.



326
 327 **Fig. 5:** The median number size distributions of small ions between 0.8 and 2.0 nm grouped by
 328 percentiles of neutral sulfuric acid concentration (a) negative and b) positive ions) and scatter plots
 329 and Spearman correlation coefficients (r_s) of hourly mean diameter of small ions (d_{mean}) and sulfuric
 330 acid concentration (c) negative and d) positive ions) in Hyytiälä. In the scatter plot, the color
 331 indicates the respective NPF rank of the day. Only daytime (10:00-16:00) values are included. The
 332 percentile values for sulfuric acid are 20%: $4.22 \cdot 10^4 \text{ cm}^{-3}$, 40%: $1.79 \cdot 10^5 \text{ cm}^{-3}$, 60%: $5.06 \cdot 10^5 \text{ cm}^{-3}$
 333 and 80%: $1.08 \cdot 10^6 \text{ cm}^{-3}$.

334 **3.3 Relationship of small ion size distribution with low volatility vapors**
 335 **in Beijing**



336
 337 **Fig. 6:** (a) Small ion median daytime (08:00-16:00) number size distributions in Beijing, grouped
 338 by percentiles of sulfuric acid (SA), SA dimer or total oxidized organic molecule (OOM)
 339 concentrations. (b) Hourly daytime mean diameter (d_{mean}) of small ions versus SA, SA dimer and
 340 total OOM concentrations. Figures i-iii are for negative polarity and figures iv-vi for positive and
 341 the figures with SA, SA dimer, and OOMs are in the respective order. Spearman correlation
 342 coefficients (r_s) are included. The percentile limits of SA, SA dimer and total OOM are 20%:
 343 $1.64 \cdot 10^6$, $1.26 \cdot 10^4$, and $2.19 \cdot 10^7$ cm⁻³; 40%: $2.53 \cdot 10^6$, $3.11 \cdot 10^4$, and $5.89 \cdot 10^7$ cm⁻³;
 344 60%: $3.66 \cdot 10^6$, $6.01 \cdot 10^4$ and $1.23 \cdot 10^8$ cm⁻³; and 80%: $5.17 \cdot 10^6$, $1.32 \cdot 10^5$, and $2.15 \cdot 10^8$ cm⁻³.

345 Fig. 6a shows the number size distributions of small ions grouped by percentiles of neutral sulfuric
 346 acid, sulfuric acid dimer and total oxidized organic molecule (OOM) concentration in Beijing. We
 347 can see that, especially compared to results already for Hyytiälä, the differences in the size

348 distributions with respect to the different values of sulfuric acid or OOMs are small for both
349 polarities. The concentration of negative ions below approx. 1.2 nm slightly decreases with
350 increasing sulfuric acid (Fig. 6a, I), or sulfuric acid dimer (Fig. 6a, ii), concentration, while the
351 concentrations above approx. 1.2 nm increase, indicating a weak but positive relationship between
352 the sulfuric acid and the negative small ion growth. Close to 2.0 nm, where the increase is the
353 highest, the concentration of negative ions is higher by around a factor of two when sulfuric acid
354 concentration is in the 80-100% percentile compared to when it is in the 0-20% percentile (Fig. 6a,
355 i). For both polarities, the concentrations below approx. 1.75 nm appear higher when the total OOM
356 concentration is in the 80-100% percentile compared to other times (Fig. 6a, iii and vi). However,
357 the concentrations close to 2.0 nm are not simultaneously higher, indicating that despite the
358 increased concentration of the small ions, a larger number of them is not growing into intermediate
359 ions.

360 Fig. 6b shows the scatter plots of d_{mean} and sulfuric acid, sulfuric acid dimer and total OOM
361 concentrations. A weak positive correlation is seen, and the Spearman correlation coefficients (r_s)
362 are between 0.08 and 0.25. The differences in the values of d_{mean} are small. The relationship between
363 the small ion size distribution or d_{mean} and the low volatility vapor concentrations in Beijing appears
364 weaker compared to Hyytiälä.

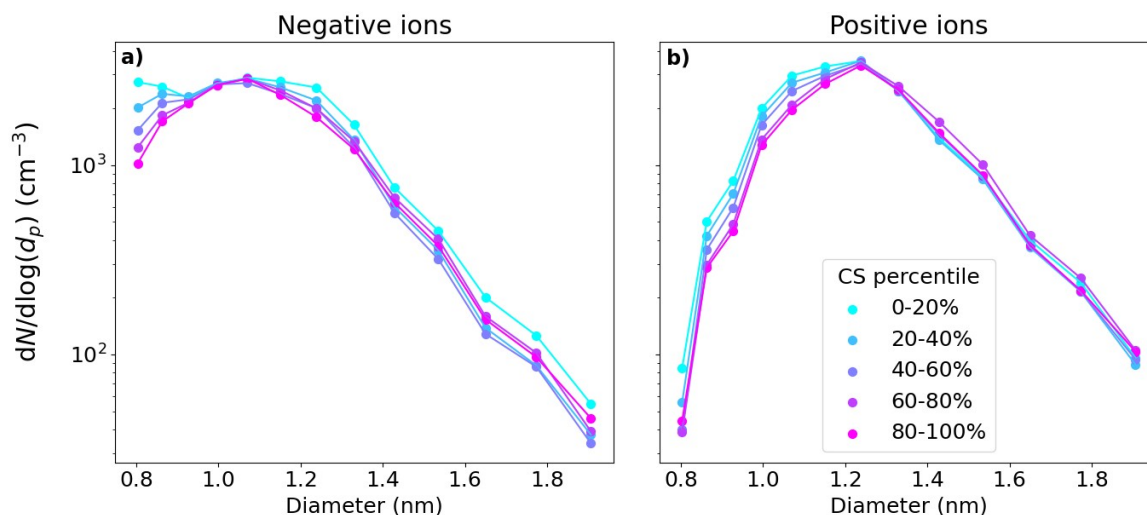
365 **3.4 Impact of coagulation scavenging on the small ion size distribution**

366 Fig. 7 shows the median small ion number size distributions in Hyytiälä and Beijing corresponding
367 to the respective percentile values of condensation sink (CS). We see that the changes in the small
368 ion size distribution with respect to changing CS are relatively small. In Hyytiälä (Fig. 7a, b), the
369 concentration of small ions, especially that of the smallest in diameter, decreases slightly with an
370 increasing CS. The sink is relatively low in Hyytiälä, and therefore this result is not unexpected.

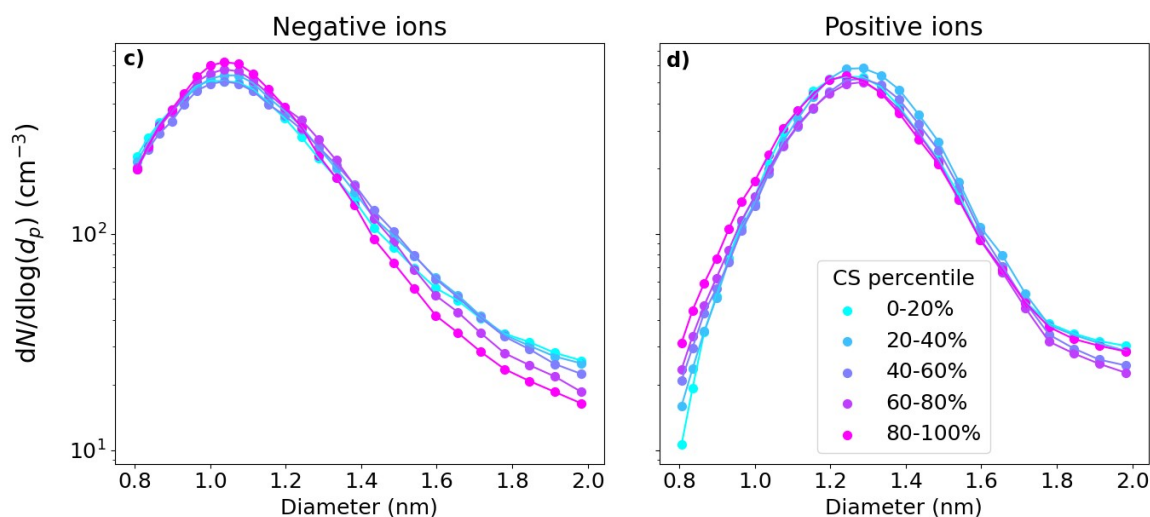
371 Based on Fig. A1, which shows the approximate values of the different terms in Eq. 2, we would
372 expect CoagS to have a much stronger impact on the small ion dynamics in Beijing than in
373 Hyytiälä. The impact should be most clear for the smallest diameters. Surprisingly, this was not
374 observed. Fig. 7c shows that in Beijing, the negative small ion size distribution below approx. 1.3
375 nm stays unchanged and the concentrations above decrease with an increasing CS. The larger
376 positive small ion concentrations (Fig. 7d) also seem to slightly decrease with increasing sink, while
377 the concentrations of the small ions close to 0.8 nm actually increase. Fig. A2a also shows that the
378 total sub-2 nm concentration barely changes with a changing CS. These results suggest that there
379 could be a source of unknown nature for small ion cluster formation that is higher when CS is high,
380 which would compensate for the increased coagulation scavenging of the ions.

381 Fig. A2d-f show the concentrations of the different low volatility vapors as a function of CS. We see
382 that the concentration of sulfuric acid (Fig. A2d) and sulfuric acid dimers (Fig. A2e) decreases with
383 an increasing sink, as expected. However, the concentration of OOMs (Fig. A2f) increases with an
384 increasing sink. While this is purely speculation, if organic compounds are forming small ion
385 clusters when the sink is higher, the weak apparent impact of CS on the small ion size distribution
386 could be explained. Alternative potential explanation could be if there is a positive correlation
387 between CS and the concentration of bases, which stabilize the small clusters. Regardless, the
388 impact of CS on the statistics of the small ion size distribution in Beijing appears very small.

Hyytiälä | 10:00-16:00



Beijing | 08:00-16:00



389

390 **Fig. 7:** the median small ion size distributions grouped by the respective percentile of the
 391 condensation sink (CS) values for Hyytiälä (a,b) and Beijing (c, d). The percentile value limits for
 392 CS for Hyytiälä are $1.3 \cdot 10^{-3} \text{ s}^{-1}$, $2.3 \cdot 10^{-3} \text{ s}^{-1}$, $3.5 \cdot 10^{-3} \text{ s}^{-1}$, and $5.5 \cdot 10^{-3} \text{ s}^{-1}$. For Beijing, the percentile
 393 value limits for CS are $9.3 \cdot 10^{-3} \text{ s}^{-1}$, $1.9 \cdot 10^{-2} \text{ s}^{-1}$, $3.1 \cdot 10^{-2} \text{ s}^{-1}$, and $4.5 \cdot 10^{-2} \text{ s}^{-1}$.

394 3.5 Correlation of small ion size distribution with sulfuric acid clusters 395 and NPF in Hyytiälä

396 Fig. 8a shows the median number size distribution of negative small ions grouped by the percentiles
 397 of the signals of SA ion clusters HSO_4^- (monomer), $\text{H}_2\text{SO}_4 \cdot \text{HSO}_4^-$ (dimer) and $(\text{H}_2\text{SO}_4)_2 \cdot \text{HSO}_4^-$
 398 (trimer) and their ratios in Hyytiälä. The median distributions are determined from daytime (10:00-
 399 16:00) values. We observe a clear increase in the number of small ions with diameters above
 400 approx. 1.2 nm with an increased signal of SA ion monomers (Fig. 8a, i) and dimers (Fig. 8a, ii).
 401 The increase is especially clear for dimers and the dimer to monomer ratio (Fig. 8a, iv), and the
 402 concentration of small ions close 2.0 nm, where the differences are highest, is an order of
 403 magnitude higher when dimer signal is in the 80-100% percentile compared to when the signal is in

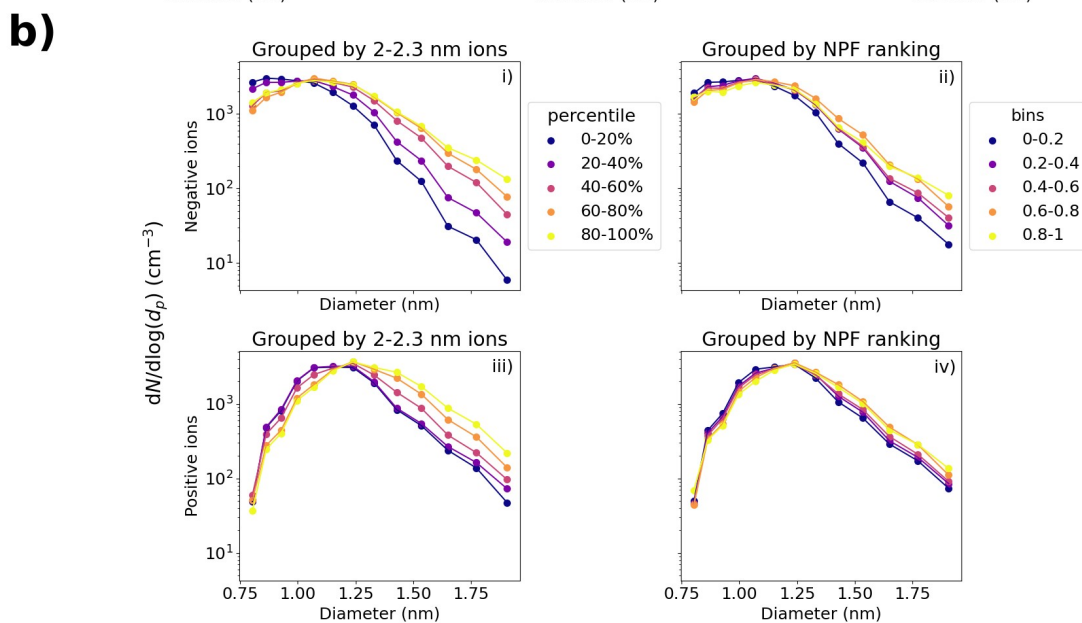
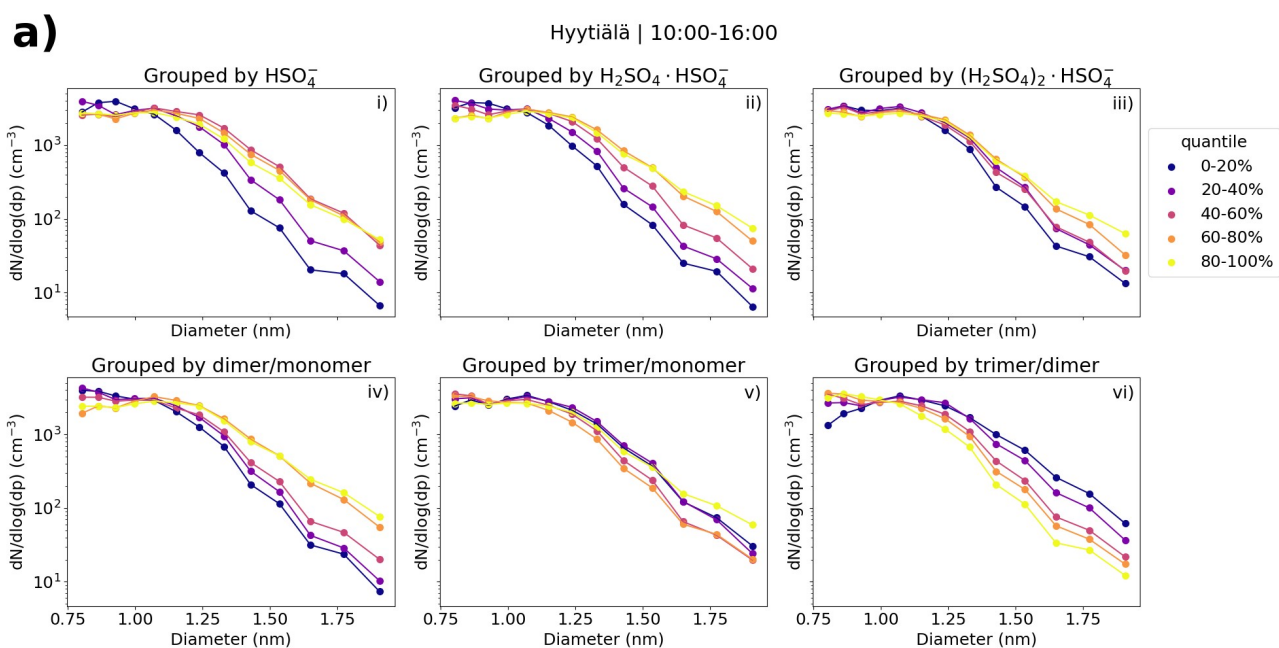
404 the 0-20% percentile. These results show that the dimer signal is a strong indicator for both the
405 cluster formation and the growth of clusters to larger sizes in Hyytiälä.

406 We used the 2.0-2.3 nm ion concentrations and NPF ranking (Aliaga et al., 2023) as proxies for
407 conditions that were favorable for cluster formation and growth. Fig. 8b shows the median daytime
408 (10:00-16:00) size distributions for both polarities with respect to the percentiles of 2.0-2.3 nm ion
409 concentrations and bins of NPF ranking in Hyytiälä. When the 2.0-2.3 nm ion concentration is
410 higher, a clear increase in concentrations is seen above approx. 1.2 nm (Fig. 8b,i and iii). The
411 difference in negative small ion concentrations close to 2.0 nm between 80-100% and 0-20% is over
412 one order of magnitude (Fig. 8b, i). The small ion size distribution for both polarities shows this
413 growth of small ions up to 2.0 nm, when local-scale intermediate ion formation is taking place.

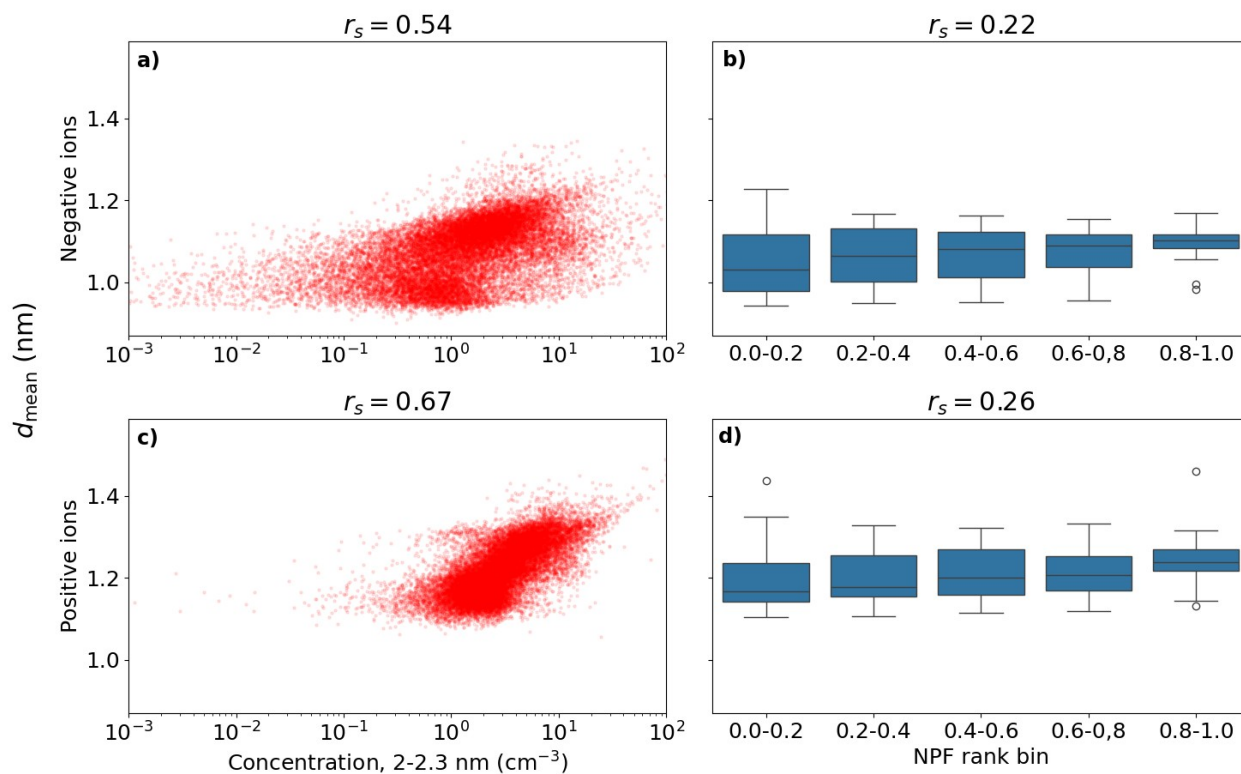
414 Similar observations can be made from the small ion size distributions with respect to the different
415 NPF ranking values. However, the differences are smaller than with respect to 2.0-2.3 nm ions, and
416 especially for positive small ions such differences are very small (Fig. 8b, iv). There is likely a
417 combination of factors at play here. First of all, NPF ranking was determined for total particles
418 between 2.5 and 5 nm and there might be differences stemming both from the ranking being less
419 sensitive for local NPF, and for 2.0-2.3 nm ion concentrations being more sensitive for ion-induced
420 clustering or NPF. In addition, differences between what is observed in the total particles versus
421 ions can be caused by variation in the chemical compounds, which take up the available charges
422 (Bianchi et al., 2017).

423 We note that the differences in the number size distribution of positive small ions are once again
424 smaller than for negative small ions. Similarly to Sect. 3.2.1, we hypothesize that this is due to the
425 size difference between the polarities.

426 Fig. 9 shows the scatter plot of hourly daytime negative (a) and positive (c) small ion d_{mean} and the
427 concentration of 2.0-2.3 nm ions. As expected, a strong positive trend is seen between d_{mean} and 2.0-
428 2.3 nm ion concentrations. The correlation coefficient is $r_s = 0.54$ (0.67) for negative (positive) ions.
429 Fig. 9 also shows the box plots of d_{mean} with NPF ranking, with negative small ions in Fig. 9b and
430 positive in 9d. The median of d_{mean} increases with increasing NPF ranking, as expected. However,
431 the variance for lower rankings is much higher, resulting in overall quite a low correlation between
432 d_{mean} and NPF ranking, $r_s =$ for negative (positive small) ions.



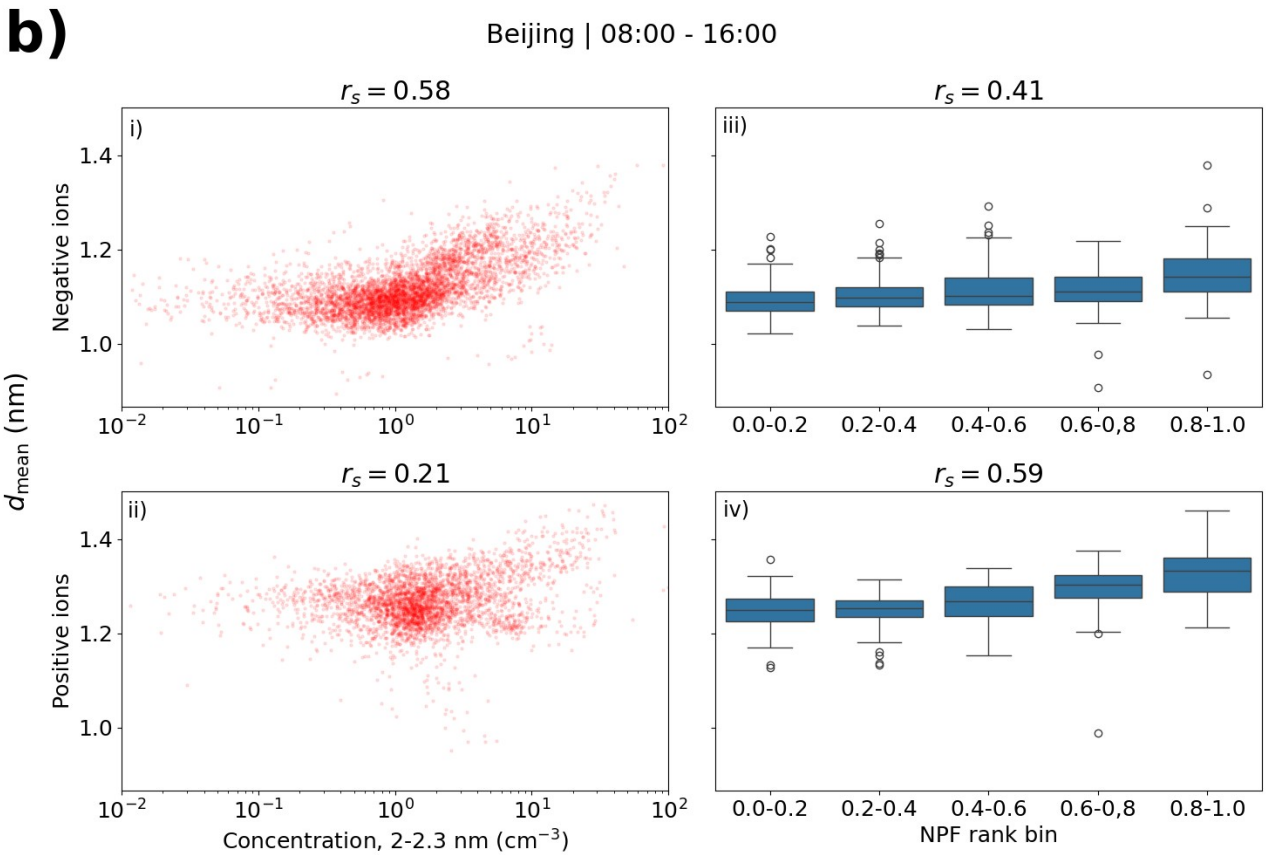
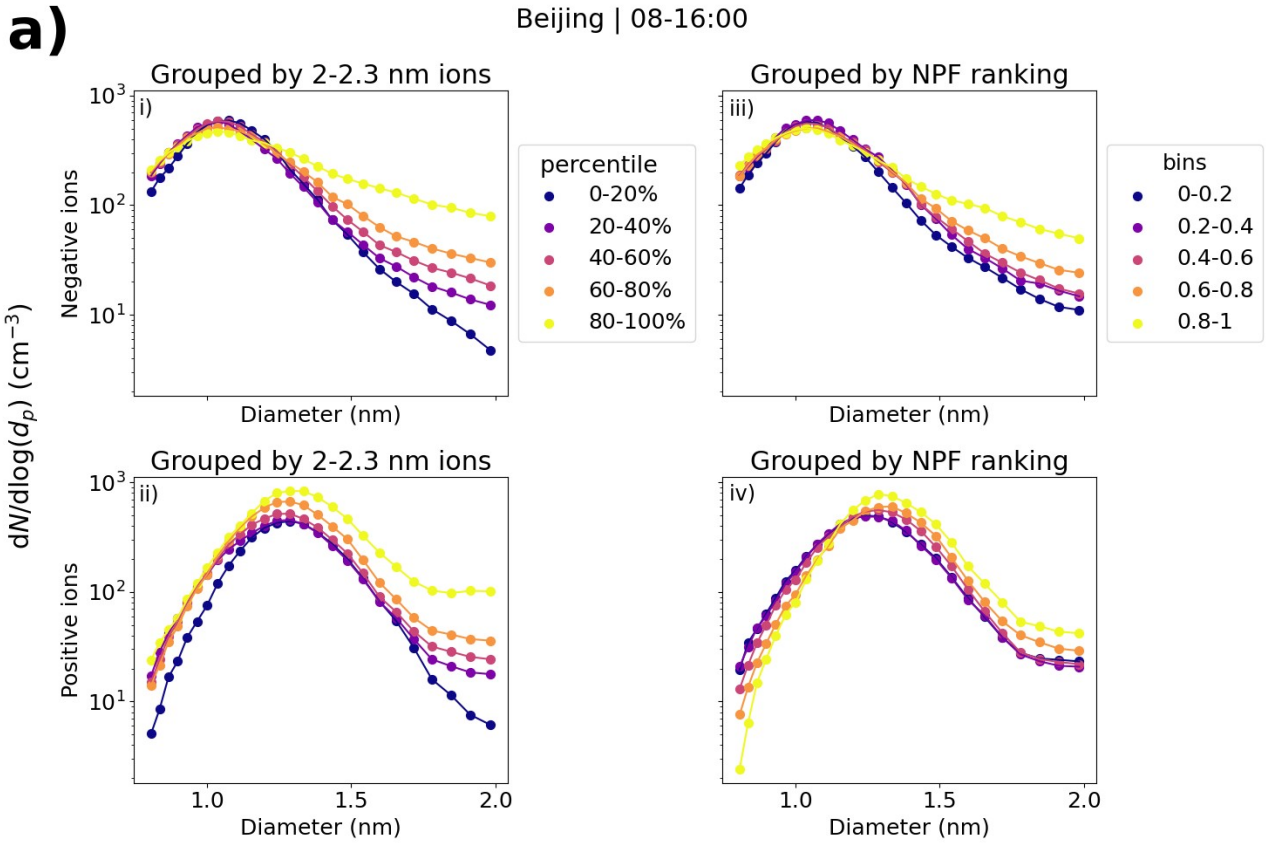
433
 434 **Fig. 8:** (a) Hyttiälä daytime median negative small ion number size distributions grouped by
 435 percentile of the signals of HSO_4^- , $\text{H}_2\text{SO}_4 \cdot \text{HSO}_4^-$ or $(\text{H}_2\text{SO}_4)_2 \cdot \text{HSO}_4^-$ ions (figures i, ii, iii,
 436 respectively) and their ratios (figures iv-vi). (b) Daytime median small ion size distributions for
 437 both polarities grouped by the percentile of 2.0-2.3 nm ion concentrations (figures i, iii) of the
 438 respective polarity or by NPF ranking (figures ii, iv). The percentile limits for negative (positive)
 439 2.0-2.3 nm ion concentrations are 20%: 0.48 (1.75) cm^{-3} , 40%: 1.01 (2.34) cm^{-3} , 60%: 1.94 (3.49)
 440 cm^{-3} , and 80%: 3.39 (5.35) cm^{-3} .



441
 442 **Fig. 9:** Hourly daytime negative (a,b) and positive (c, d) small ion diameter versus concentration of
 443 2.0-2.3 nm ions of respective polarity (a, c) or NPF ranking (b, c) in Hyytiälä. Correlation
 444 coefficients (r_s) are also shown. The middle line of the box plots for d_{mean} and NPF rank are the
 445 median values, while the boxes show the 25% and 75% percentiles and the lines the 10% and 90%
 446 percentiles.

447 **3.6 Impact of NPF on small ion distribution in Beijing**

448



449

450 **Fig. 10:** (a) Median negative and positive small ion number size distributions in Beijing grouped by
451 percentiles of 2.0-2.3 nm ion concentrations (b). Scatter plots of mean diameter and 2.0-2.3 nm ion
452 concentrations (of respective polarity) or NPF ranking. Figures. i-ii are for negative polarity and iii-
453 iv for positive. Values are for daytime (08:00-16:00). The percentile limits of 2.0-2.3 nm
454 concentration for negative (positive) ions are 20%: 0.51 (0.85) cm^{-3} , 40%: 0.92 (1.27) cm^{-3} , 60%:
455 1.33 (1.72) cm^{-3} , and 80%: 2.47 (3.22) cm^{-3} .

456
457 Fig. 10a shows the small ion size distributions with respect to the concentration of 2.0-2.3 nm ions
458 (i, ii) or NPF ranking (iii, iv) in Beijing. Negative ions are in Figures i-ii and positive in Figures iii-
459 iv. For both polarities, clear differences are seen in the distributions depending on the percentile of
460 the 2.0-2.3 nm ion concentration. When the 2.0-2.3 nm ion concentrations are higher, the
461 concentration of negative (positive) small ions above approx. 1.0 (1.3) nm is increased. The
462 differences are largest close to 2.0 nm. Comparing the 0-20% and 80-100% percentiles, the
463 difference in the concentrations is around one order of magnitude when the diameter is approaching
464 2.0 nm, comparable to what was observed in Hyytiälä. Similar observations are seen with respect to
465 NPF ranking, although to a lesser extent. For negative small ions (Fig. 10a, ii), the concentration at
466 around 2.0 nm is four to five times higher when the NPF ranking is above 0.80 compared to when it
467 is below 0.20. For positive ions, the concentration is less than two times higher (Fig. 10a, iv).

468
469 When looking at the small ion distributions in Beijing with respect to different 2.0-2.3 nm ion
470 concentrations or NPF ranking, unlike for low-volatility vapor concentrations, we are able to see the
471 growth of small ions to intermediate ions in the size distribution. These results show that the growth
472 of small ions to larger diameters in Beijing is not limited by the availability of sulfuric acid or
473 oxidized organic vapors, unlike in Hyytiälä. In addition, based on our analysis it does not appear to
474 be strongly limited by CS either. This is supported by the relatively weak correlation between CS
475 and the NPF ranking or 2.0-2.3 nm ions (Fig. A2b,c). Therefore, we speculate that the small ion
476 growth could be limited more by the availability of bases. However, due to the lack of long-term
477 base concentration data, this question remains unanswered.

478
479 Fig. 10b shows the scatter plots of d_{mean} and 2.0-2.3 nm ion concentration and the box plots of d_{mean}
480 and NPF ranking. The correlation coefficients for negative ions are as expected, $r_s = 0.58$ and $r_s =$
481 0.41 between d_{mean} and 2.0-2.3 nm ion concentration or NPF ranking, respectively. For positive ions,
482 the correlation coefficient between d_{mean} and NPF ranking is $r_s = 0.59$, while it is only 0.21 between
483 d_{mean} and 2.0-2.3 nm ion concentration. From Fig. 10a we see that the concentrations of positive
484 small ions below 1.0 nm also increase to some extent with increasing 2.0-2.3 nm ion concentration,
485 which likely impacts the values of d_{mean} , resulting in a relatively poor overall correlation.

486
487 Notably, the differences in the size distributions with respect to NPF ranking are clearer and the
488 correlation between d_{mean} and the ranking is stronger in Beijing than in Hyytiälä for both polarities.
489 One of the explaining factors could be the fact that intense NPF in Beijing is more common than in
490 Hyytiälä (e.g., Dada et al., 2017; Deng et al., 2020), impacting the statistics of the ranking. Another
491 possibility is that local clustering events, where ions or particles grow close to 2.0 nm but not much
492 further, could be more common in Hyytiälä.

493

494 **3.7 Case studies**

495 Next, some case studies into the development of negative small ion size distributions, and other
496 investigated variables, are presented for Hyytiälä and Beijing. These cases show that we are able to
497 observe the cluster growth, driven by daytime NPF or evening clustering, from the ion number size
498 distributions of individual days and not only from the statistics of the size distributions. Based on

499 the analysis presented in this study, the behavior of negative and positive small ion populations is
500 mostly similar, and therefore, for simplicity, we have limited the analysis here to negative polarity.

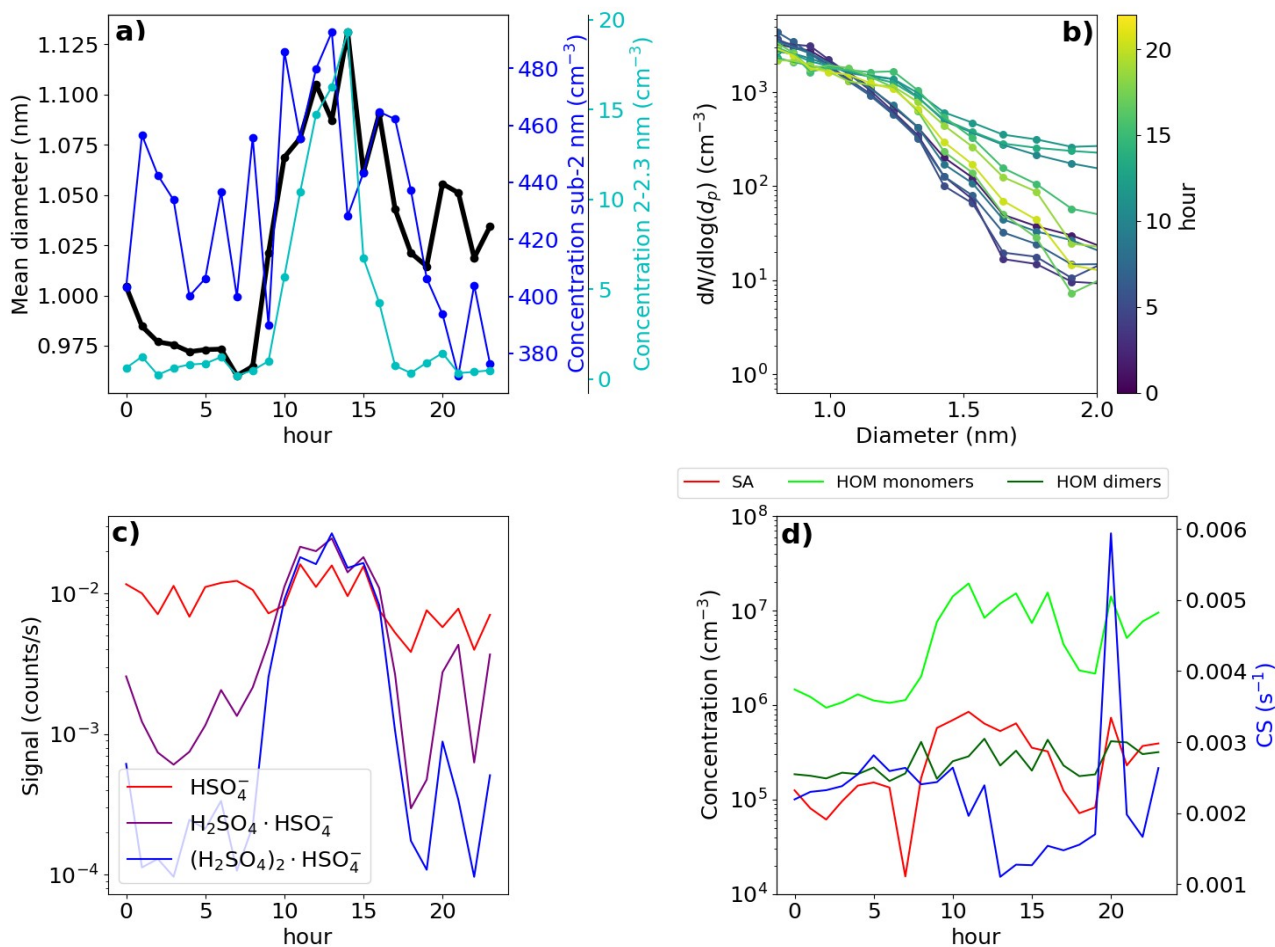
501 **3.7.1 Hyytiälä case 1 – an early spring day with NPF**

502 First of the investigated days was 10th of March, in 2021 and is presented in Fig. 11. During this
503 day, a strong NPF event was observed with clear growth observed both in the total particle and ion
504 number size distribution (see Fig. A3). In the morning, a strong increase in the SA ion dimer and
505 trimer signals was detected after 07:00 (Fig. 11c), which occurred simultaneously with an increase
506 in the concentration of neutral sulfuric acid. Shortly after, at around 08:00, neutral HOM monomer
507 concentration started to increase (Fig. 11d). A strong increase in the concentration of 2.0-2.3 nm
508 negative ions was observed after 09:00, indicating intense NPF on a local-scale (Fig. 11a).
509 Approximately one hour before an increase in the concentration of 2.0-2.3 nm ions was first
510 observed, the small ion d_{mean} started to increase from below 1.0 nm (Fig. 11a), showing that growth
511 of clusters in the small ion population to larger sizes had begun. We can also see this from the
512 negative ion number size distributions (0.8-2.0 nm; Fig. 11b): in the early hours of the day, the
513 concentrations of the smallest ions are at their highest while the concentration of ions above approx.
514 1.1 nm are at their lowest. Throughout the morning hours, we can see that the concentration of ions
515 above approx. 1.1 nm increases and in the afternoon, around 14:00, the concentration of ions close
516 to 2.0 nm is over a order of magnitude higher than during the night before. At around 14:00, the
517 concentration of 2.0-2.3 nm ions and small ion d_{mean} also reach their peaks. At the same time, CS is
518 at its lowest (Fig. 11d). Then, the concentrations of larger small ions, 2.0-2.3 nm and SA ion
519 clusters starts to decrease, alongside with the concentration of HOM monomers.

520 We also took a look at the diameter specific concentrations in a smaller time frame (Fig. A6), which
521 clearly shows how clear increase concentrations is observed for the diameters above 1.2 nm. A time
522 delay between the increasing concentration of larger ions and smaller ions was seen, showing the
523 growth of ions between 1.2 to 2.0 nm. Using the appearance time method (Lehtipalo et al., 2014),
524 GR between 1.24 to 2.05 nm was estimated: GR = 0.40 nm/h. This value is somewhat lower than
525 typical GRs reported in Hyytiälä (Hirsikko et al., 2005; Yli-Juuti et al., 2011), as expected due to
526 the small size of the considered ions. Regardless, it shows that the growth of ions below 2.0 nm is
527 non-negligible on this particular day. We note that this GR, or the ones presented for Hyytiälä Case
528 2 and Beijing Case, is not a representative of the whole range of GRs for similar cases in the same
529 location, and that there can be considerable variability.

530 This day clearly shows how the sulfuric acid and HOM driven particle formation is seen as the
531 growth of the small ions to larger diameters. With the ion size distribution data, we have been able
532 to get insight on when the cluster growth starts and how it progresses throughout this day.

2021-03-10



533
534
535
536
537
538
539

Fig. 11: Data from Hyytiälä, 10th of March, 2021. (a) Hourly mean diameter of negative small ions (0.8-2.0 nm), total concentration of small ions, and concentration of 2.0-2.3 nm negative ions. (b) Two-hour median number size distribution of negative small ions. (c) Hourly signals of HSO₄⁻, H₂SO₄·HSO₄⁻ and (H₂SO₄)₂·HSO₄⁻ ions. (d) Hourly median concentrations of neutral sulfuric acid (SA) and highly oxidized molecule (HOM) monomers and dimers, and the condensation sink (CS).

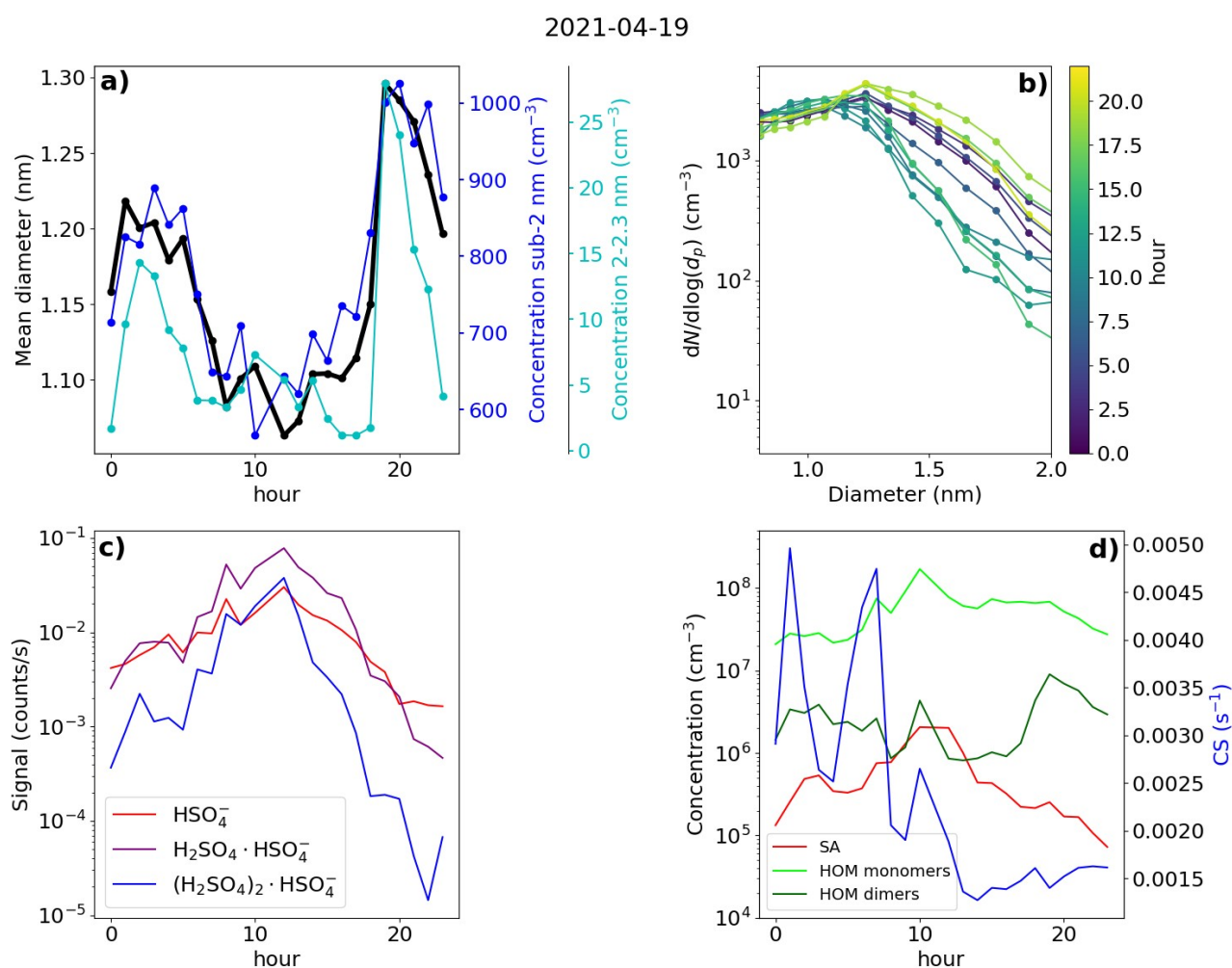
540 3.7.2 Hyytiälä Case 2 – a spring day with strong evening clustering

541 The second of the chosen days for Hyytiälä is 19th of April, 2021 (Fig. 12). The NPF ranking of this
542 day was high, over 0.9, however the growth in the negative ion and total particle mode was
543 discontinuous with the clearest growth observed above 5.0 nm, suggesting that the fraction of
544 growing locally formed neutral clusters or ions was low (Fig. A4). However, strong evening ion
545 cluster formation was observed on this day. Therefore, Case 2 illustrates both the contribution of
546 organic vapors to initiate the growth of larger particles and the evening ion cluster formation
547 attributable to HOM dimers (Mazon et al., 2016).

548 Starting from the early hours of the day, the signals of SA ions and neutral SA concentration
549 increase (Fig. 12c and 12d), reaching their maxima around 13:00 in the early afternoon. Compared
550 to Hyytiälä Case 1, the signal from trimers is lower in relation to the signal from monomer and
551 dimer. At the same time, CS decreases (Fig. 12d). From the negative ion number size distributions
552 (Fig. 12b), we see that the concentration of negative ions below approx. 1.2 nm increases and the
553 concentration of small ions above approx. 1.2 nm strongly decreases starting from the early hours of

554 the day until afternoon. This is reflected in the value of d_{mean} , which decreases from over 1.2 nm to
 555 below 1.1 nm (Fig. 12a). The concentration of 2.0-2.3 nm negative ions decreases until 08:00 in the
 556 morning, after which it increases briefly before decreasing again (Fig. 12a). The small ion total
 557 concentration also strongly decreases from over 800 cm^{-3} to 600 cm^{-3} (Fig. 12a). Unlike in Case 1,
 558 on this day, the growth of small ions during daytime is negligible and an increased fraction of the
 559 available charge is taken up by small, below 1.2 nm ions, many of which are likely composed of
 560 sulfuric acid monomers or dimers. This explains the behavior of the ion size distributions, d_{mean} and
 561 the total small ion concentration.

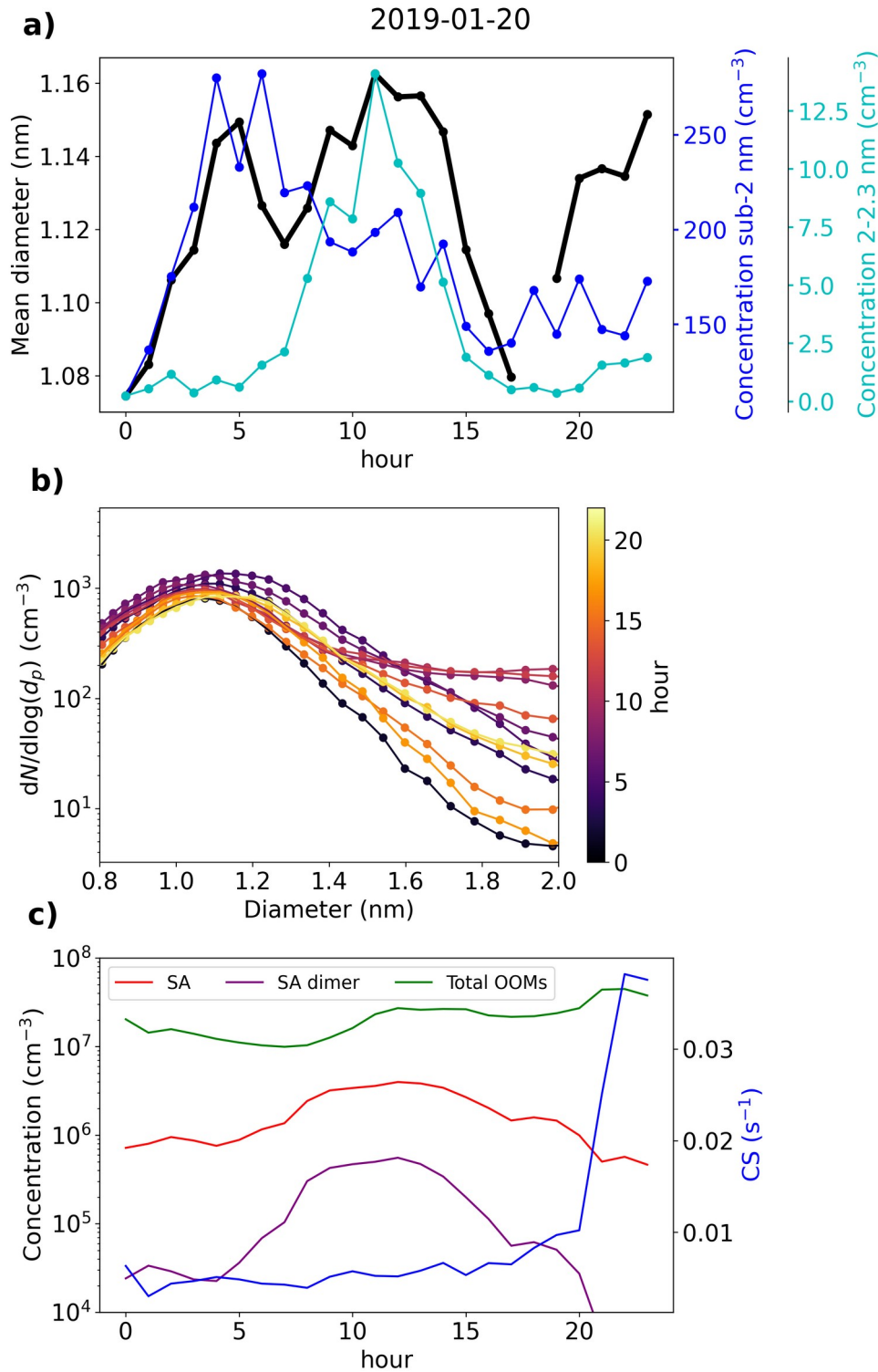
562 After 14:00 in the afternoon, the concentration of neutral HOM dimers starts to increase, and
 563 reaches a peak at around 19:00 (Fig. 12d). Compared to Case 1, the HOM dimer concentration is
 564 over one order of magnitude higher. Notably, at the same time as the HOM dimer concentration
 565 starts increase, clear growth of total particles above 5.0 nm is observed (Fig. A4). Concentration of
 566 small ions larger than approx. 1.2 nm (Fig. 12b) and 2.0-2.3 nm ion concentration (Fig. 12a)
 567 strongly increase. Small ion d_{mean} increases from approx. 1.1 nm to 1.3 nm, while the total negative
 568 small ion concentration increases from around 600 cm^{-3} to 1000 cm^{-3} . The negative ion GR between
 569 1.43 to 2.05 nm was estimated to be 1.28 nm/h (Fig. A6), which is over twice as high as the GR
 570 estimated for Case 1, likely due to the high concentration of lower volatility HOMs driving the
 571 small ion growth during this particular evening.



572
 573 **Fig. 12:** Data from Hyytiälä, 19th of April, 2021. (a) Hourly mean diameter of negative small ions

574 (0.8-2.0 nm), total concentration of small ions, and concentration of 2.0-2.3 nm negative ions. (b)
 575 Two-hour median number size distribution of negative small ions. (c) Hourly signals of HSO_4^- ,
 576 $\text{H}_2\text{SO}_4\cdot\text{HSO}_4^-$ and $(\text{H}_2\text{SO}_4)_2\cdot\text{HSO}_4^-$ ions. (d) Hourly median concentrations of neutral sulfuric acid
 577 (SA) and highly oxidized molecule (HOM) monomers and dimers, and the condensation sink (CS).

578 **3.7.3 Beijing Case – a day with intense NPF**



579

580 **Fig. 13:** Data from Beijing, 20th of January, 2019. (a) Hourly mean diameter of negative small ions
581 (0.8-2.0 nm), total concentration of small ions, and concentration of 2.0-2.3 nm negative ions. (b)
582 Two-hour median number size distribution of negative small ions. (c) Hourly median concentrations
583 of neutral sulfuric acid (SA), SA dimer, and total oxidized organic molecules (OOMs), and
584 condensation sink (CS).

585 Fig. 13 presents data from Beijing on 20th of January, 2019. This day was characterized by an
586 intense NPF event, observed both in the ion and the total particle size distribution (Fig. A5). We see
587 that from 00:00 until 05:00 in the morning, the negative small ion concentrations seem to increase,
588 which is apparent for the whole sub-2 nm size range (Fig. 13a and 13b). Simultaneously, d_{mean} of the
589 small ions increases (Fig. 13a). The concentration of 2.0-2.3 nm negative ions stays low (Fig. 13a),
590 indicating that there is no significant growth of small ions to intermediate ions. CS is similar
591 throughout the night and the early morning. Based on the data presented here, we hypothesize that
592 the increase in small ion concentration is attributed to a larger fraction of the ions being detected by
593 the instrument as d_{mean} increases.

594 After 05:00 in the morning, an increase in neutral sulfuric and sulfuric acid dimer concentration is
595 observed (Fig. 13c). Simultaneously, the concentration of 2.0-2.3 nm ions increases sharply,
596 indicating the formation of intermediate ions. Two changes in the small ion size distribution are
597 shown: first, the concentration of small ions below approx. 1.5 nm ions, decreases and second, the
598 concentration of small ions above that increases. Increasing growth of small ions to larger sizes
599 causes a shift in their size distribution. Notably, no growth in the surface plots (Fig. A5) is observed
600 yet, likely due to locality of or insufficient intensity of the ion formation. After 12:00, the
601 concentrations of small ions larger than approx. 1.5 nm start to decrease, as does the concentration
602 of 2.0-2.3 nm ions. While the growth of ions and particles at larger diameters continues, the
603 intensity of the cluster growth decreases.

604 In this case, the negative small ion GR was estimated to be 0.24 nm/h from 1.72 to 2.06 nm (Fig.
605 A7), which is lower than the values determined for the two Hyytiälä cases and is on the lower range
606 of values of particle GRs for Beijing (Deng et al., 2020). Another noteworthy observation can be
607 made from the diameter specific concentrations (Fig. A7): as already seen from the size
608 distributions and more clearly here, the concentrations of ions up to around 1.5 nm decrease, while
609 the concentrations above increase at the same time. This implies that the ions, which actually start
610 to grow to larger sizes are close to 1.5 nm in diameter, though at such a low GR their survival
611 probability to larger sizes is likely very low (Kulmala et al., 2017).

612 In Sect. 3.3, we saw how in Beijing there does not seem to be correlation between the small ion
613 number size distribution and the concentration of sulfuric acid. On this day, the increased
614 concentrations of sulfuric acid occurred approx. simultaneously with the observed small ion growth.
615 Previous studies have shown the importance of sulfuric acid in particle formation in Beijing (Yao et
616 al., 2018; Cai et al., 2021; Yan et al., 2021). As such, it seems likely that the growing small ions
617 seen on this day are composed of sulfuric acid. However, while sulfuric acid forms these growing
618 clusters, their growth also requires other ingredients.

619 **4 Conclusions**

620 We studied the seasonality of the small ion number size distribution and the relationship of the
621 small ion size distribution with low-volatility organic vapors, sulfuric acid, coagulation sink
622 (CoagS) and NPF in a rural boreal forest location of Hyytiälä, Finland and an urban megacity
623 location of Beijing, China. Both analysis of long time series of data and daily case studies were
624 carried out. We found a clear seasonality of the small ion size distribution in Hyytiälä, where the
625 small ions of both polarities were the smallest in size during winter and the largest during late
626 spring and summer. In Beijing, while there were month-to-month variations in the size distribution,
627 but no clear seasonal pattern was identified.

628 We found that in Hyytiälä the small ion size distribution strongly varied with respect to the
629 concentration of organic, especially highly oxidized organic (HOM) monomer, compounds and that
630 the concentration of small ions above approx. 1.2 nm increased strongly with increasing HOM
631 monomer concentration. This was observed more strongly for negative polarity and during the
632 evening, which was found to be connected to the evening ion cluster formation driven by organics
633 in Hyytiälä. The small ion size distribution also showed clear increase in the size of the small ions
634 in Hyytiälä with respect to neutral sulfuric acid and ionized sulfuric acid dimers, associated with
635 daytime cluster formation and growth. In contrast, there was no clear relationship between the
636 concentration of either organic vapor or sulfuric acid and the size of the small ions in Beijing. The
637 reason for this remains to be identified, but we hypothesize that the concentration of bases is the
638 limiting factor determining if growth of small ions is seen in Beijing.

639 We found that the small ion size distribution in either location did not change strongly with
640 changing CoagS. In Hyytiälä, small decrease in the concentration of especially the smallest ions
641 was seen, as expected. However, despite our expectations, this was not observed in Beijing. The
642 reason for this remains to be answered in future research.

643 When the concentration of ions in the range 2.0-2.3 nm increased, indicating the occurrence of local
644 NPF, we observed clear signs of growth in the small ion size distribution. This was seen in both
645 locations, even in Beijing, where no clear association of small ion size with organic vapor or
646 sulfuric acid was found. To a lesser extent, an increase in the small ion size was also seen with
647 respect to NPF rank, a parameter, which characterizes the intensity of NPF. These results support
648 the conclusion that in Beijing the concentration of sulfuric acid or organic vapor does not determine
649 whether small ions grow to intermediate ions.

650 Overall, we have shown in a novel way how the atmospheric cluster formation and growth
651 processes impact the number size distribution of small ions. The sub-2 nm size range is integral for
652 understanding of the first steps of new particle formation and the activation of the clusters to grow
653 into particles. Our results can be applied in research into the dynamics of charged clusters and how
654 they grow from clusters to particles.

655 **Author contributions**

656 ST analyzed the data and wrote the manuscript. JL was responsible for the ion measurements in
657 Hyytiälä. CL and NS were responsible for the measurements of low-volatility vapors and ion

658 clusters. YL was responsible for the measurements in Beijing. MK, VMK, and ST conceptualized
659 the study. All authors contributed to reviewing and editing the manuscript.

660 Code and data availability

661 The Hyytiälä DMPS dataset can be accessed through the SmartSMEAR data portal at
662 <https://smear.avaa.csc.fi/>. Other data and the codes used to produce the figures in this paper are
663 available upon request from the authors.e

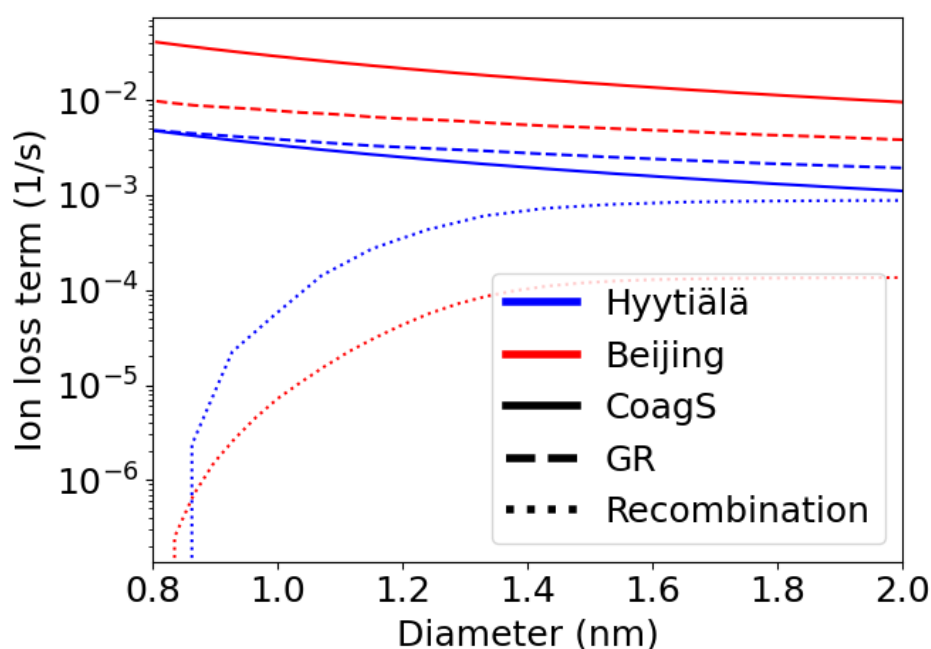
664 Competing interests

665 At least one of the (co-)authors is a member of the editorial board of Aerosol Research. Authors
666 have no other competing interests to declare.

667 Acknowledgments

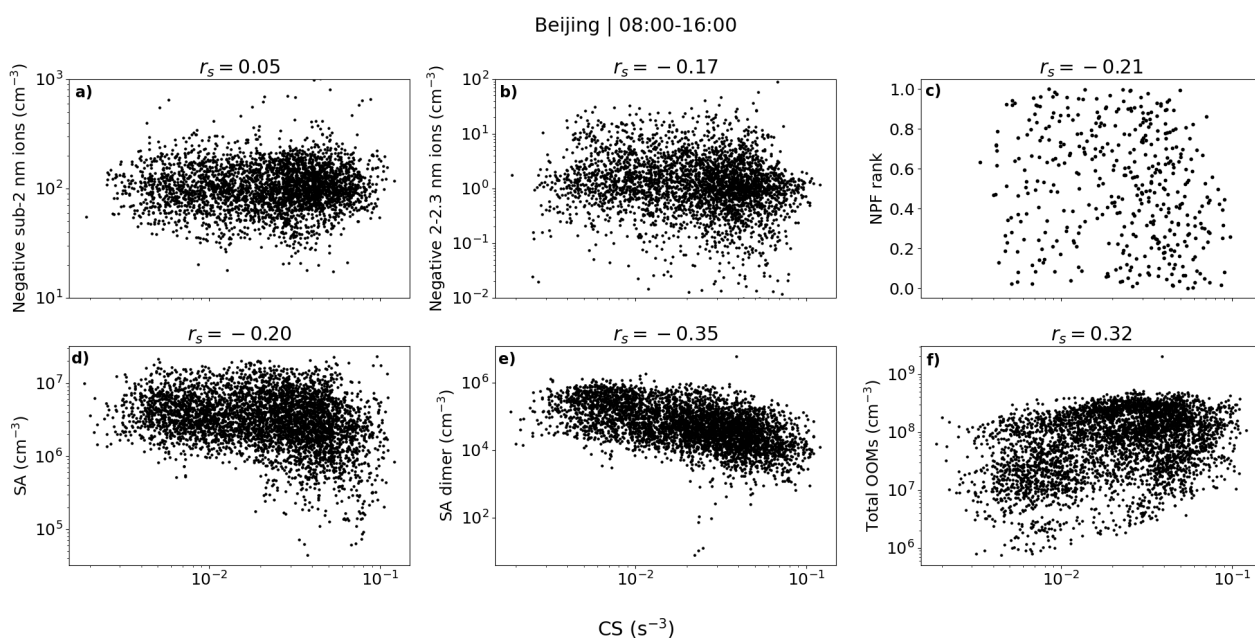
668 This work has been supported by the ACCC Flagship funded by the Academy of Finland grant nos.
669 337549 (UH) and 337552 (FMI), and the “Gigacity” project funded by the Jenny and Antti Wihuri
670 Foundation. We acknowledge the SMEAR II and AHL/BUCT technical and scientific staff.

671 Appendix



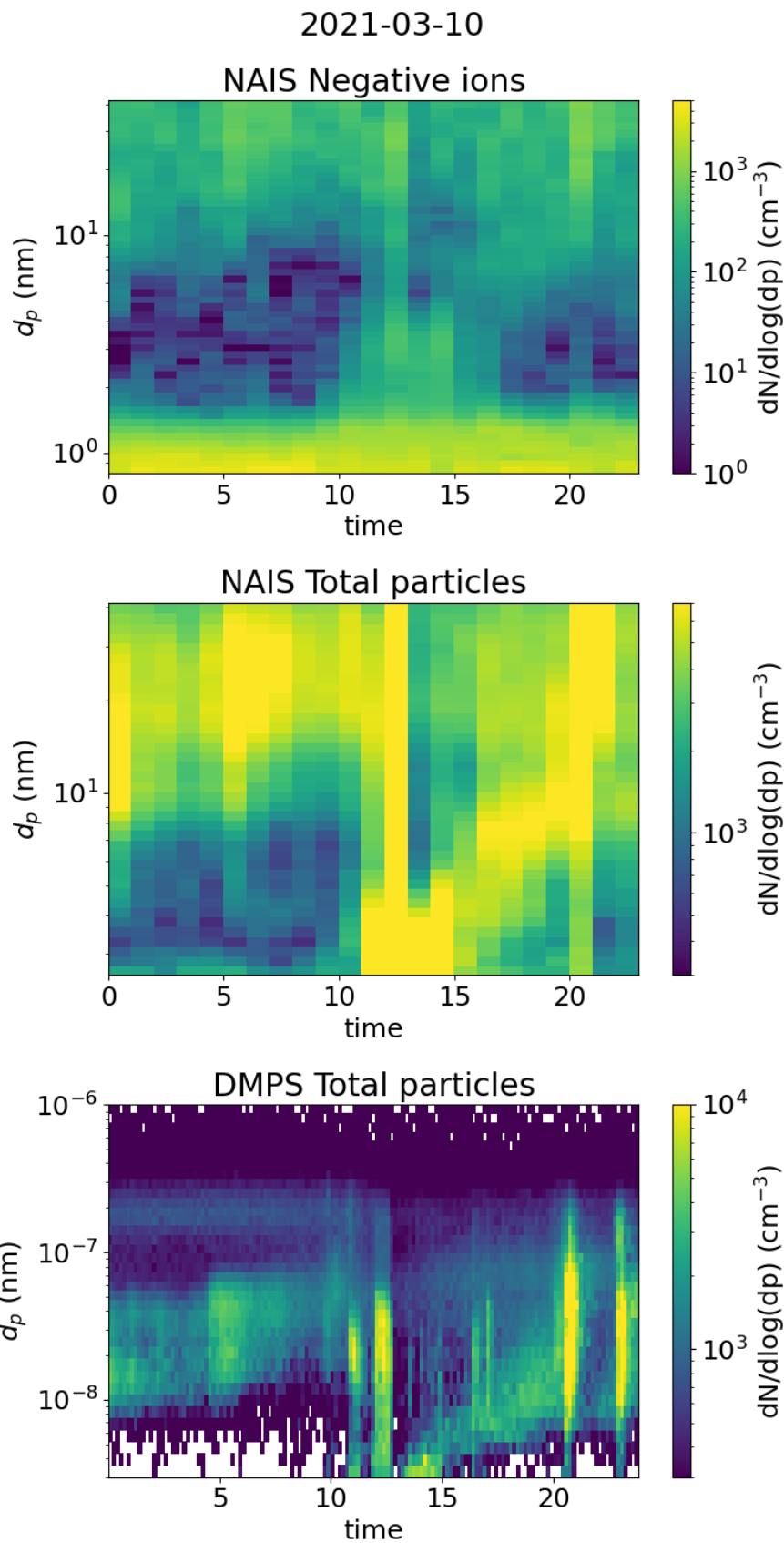
672

673 **Fig. A1:** A rough approximation of the different loss terms of negative ions as a function of ion
674 diameter based on Eq. 2 in both Hyytiälä and Beijing. The concentration of positive ions were based
675 on the median number size distributions. GR was assumed to equal 1 nm/h and was assumed to be
676 constant with diameter. CoagS was scaled based on the median CS, and assuming that the charge
677 enhancement of the sink was by a factor of 2. The median CS were $CS=2.9 \cdot 10^{-3} \text{ s}^{-1}$ and $2.5 \cdot 10^{-2} \text{ s}^{-1}$,
678 for Hyytiälä and Beijing, respectively.



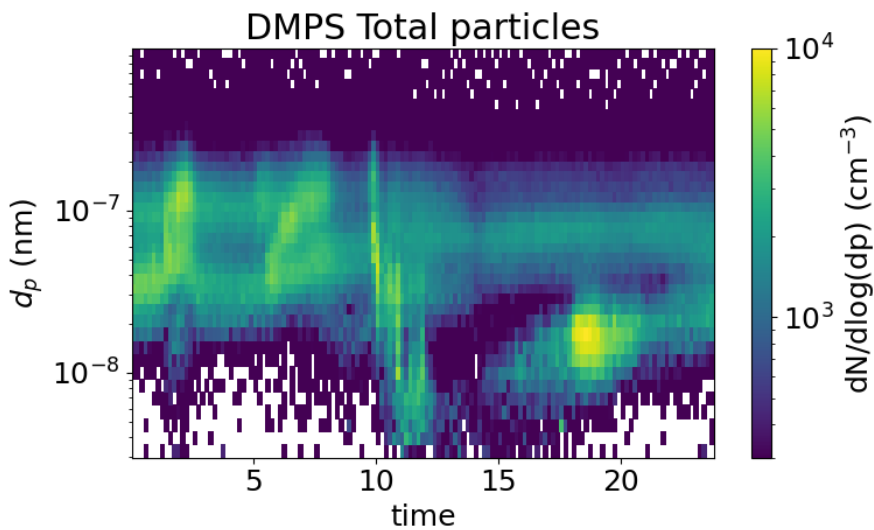
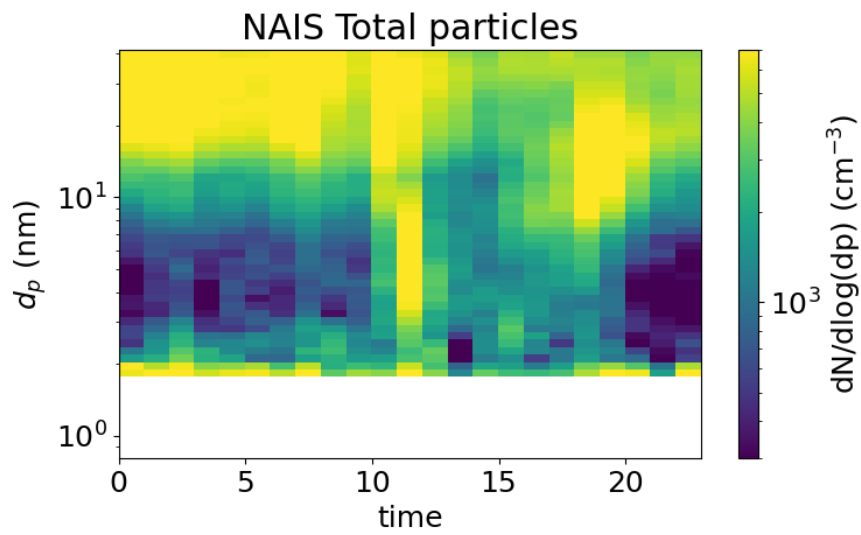
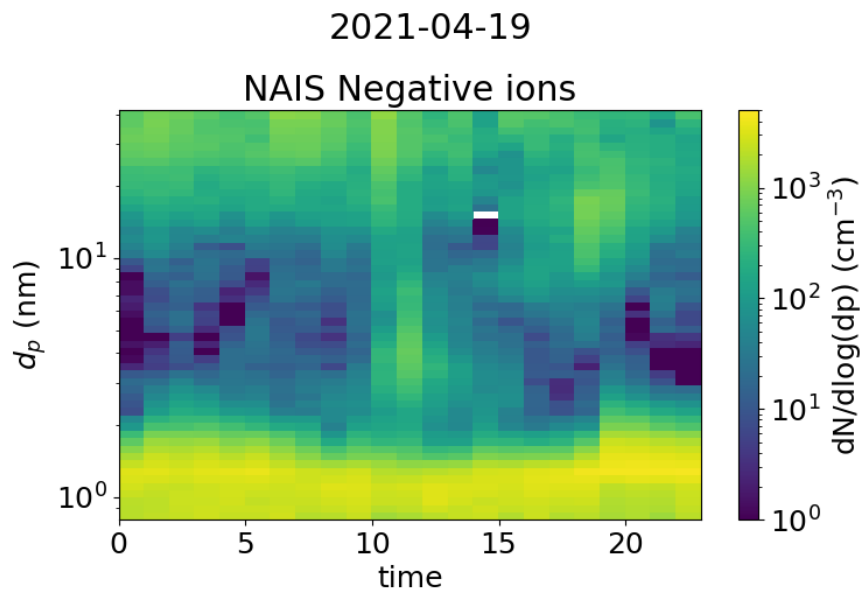
679

680 **Fig. A2:** The concentrations of negative sub-2 nm (a) and 2.0-2.3 nm (b) ions, NPF ranking values
 681 (c), and the concentrations of neutral sulfuric acid (SA, d), SA dimer (e), and total oxidized organic
 682 molecules (OOMs, f) with respect to condensation sink (CS) in Beijing. The values are hourly
 683 medians, except for c), where NPF ranking is a daily parameter and CS is the daytime median. The
 684 Spearman correlation coefficients (r_s) are also shown.



685

686 **Fig. A3:** Surface plots of negative ion number size distribution and total particle number size
 687 distribution measured by NAIS and DMPS in Hyytiälä on 10th of March, 2021.

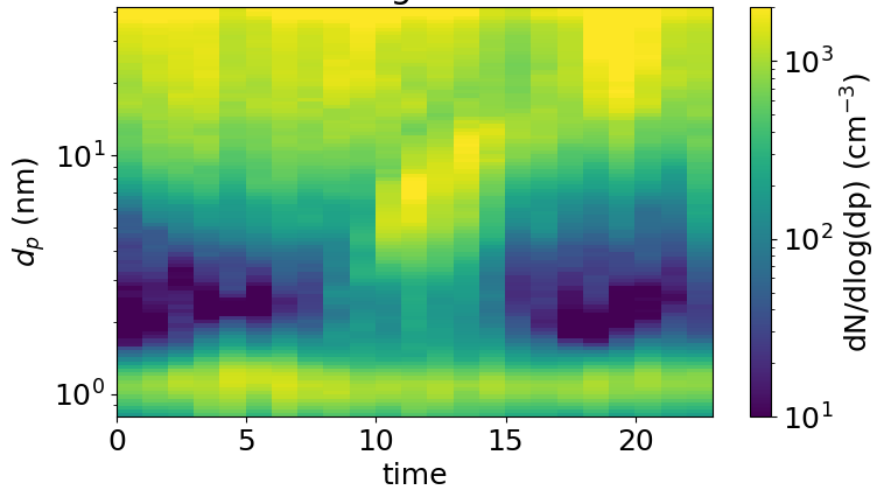


688

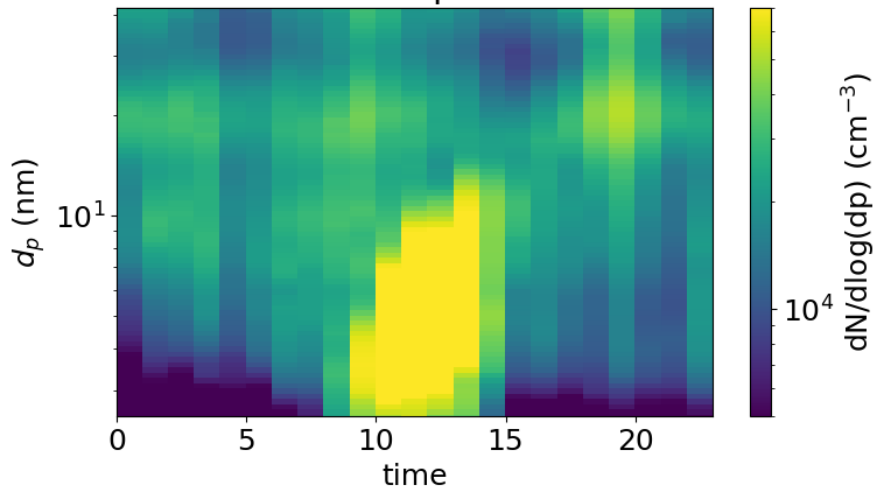
689 **Fig. A4:** Surface plots of negative ion number size distribution and total particle number size
 690 distribution measured by NAIS and DMPS in Hyytiälä on 19th of April, 2021.

2019-01-20

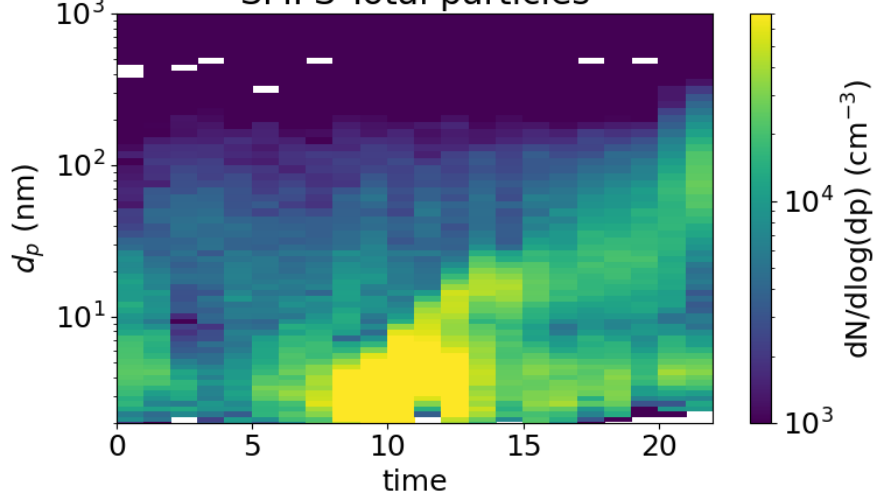
NAIS Negative ions



NAIS Total particles

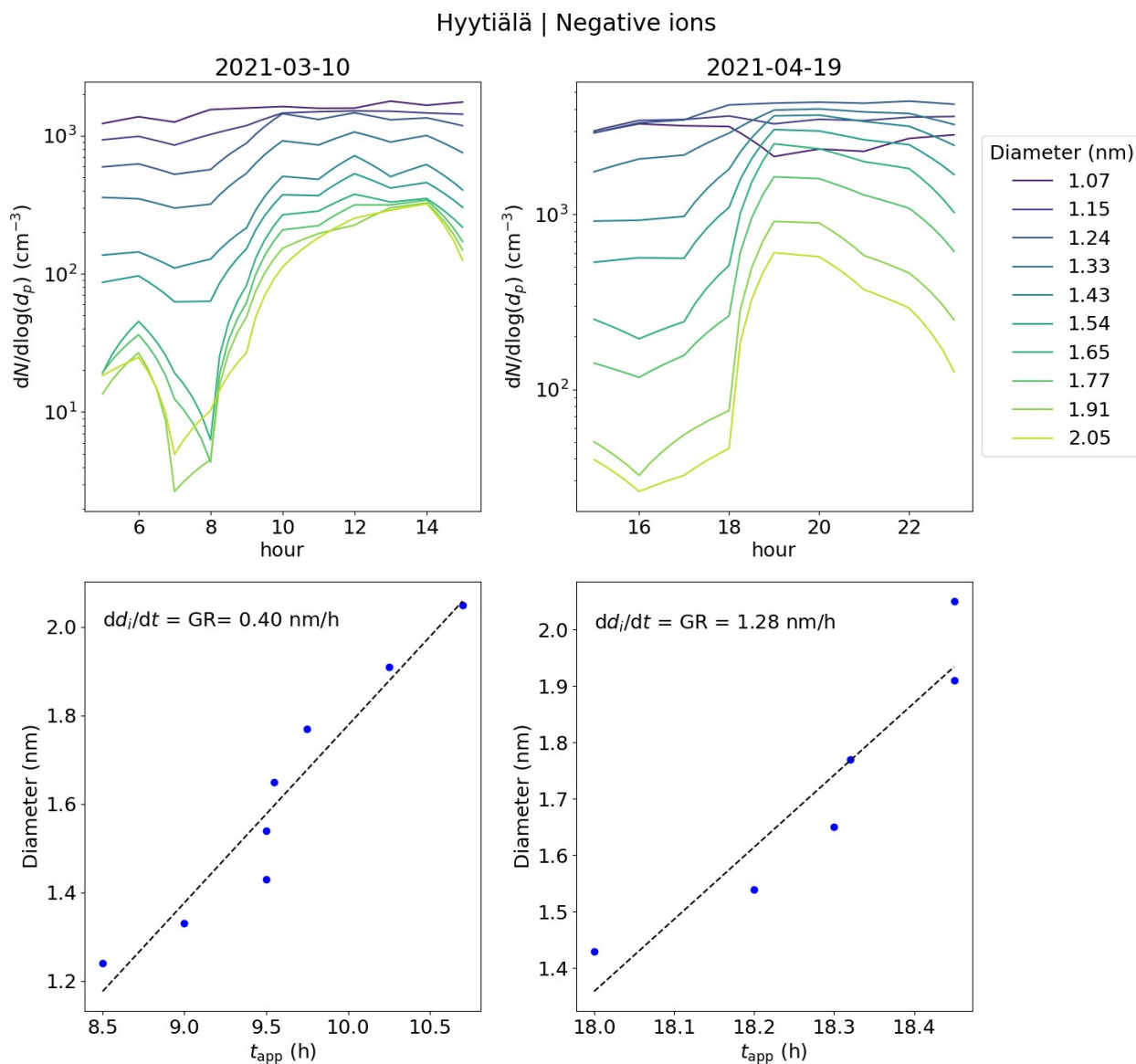


SMPS Total particles



692 **Fig. A5:** Surface plots of negative ion number size distribution and total particle number size
 693 distribution measured by NAIS and SMPS (see Liu et al., 2016 for more information) in Beijing on
 694 20th of January, 2019.

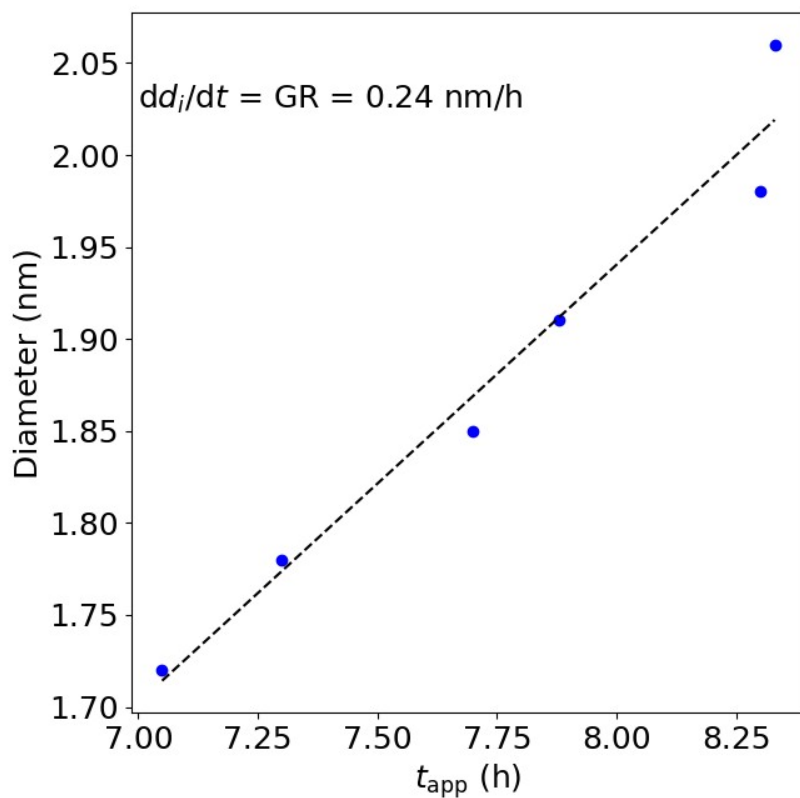
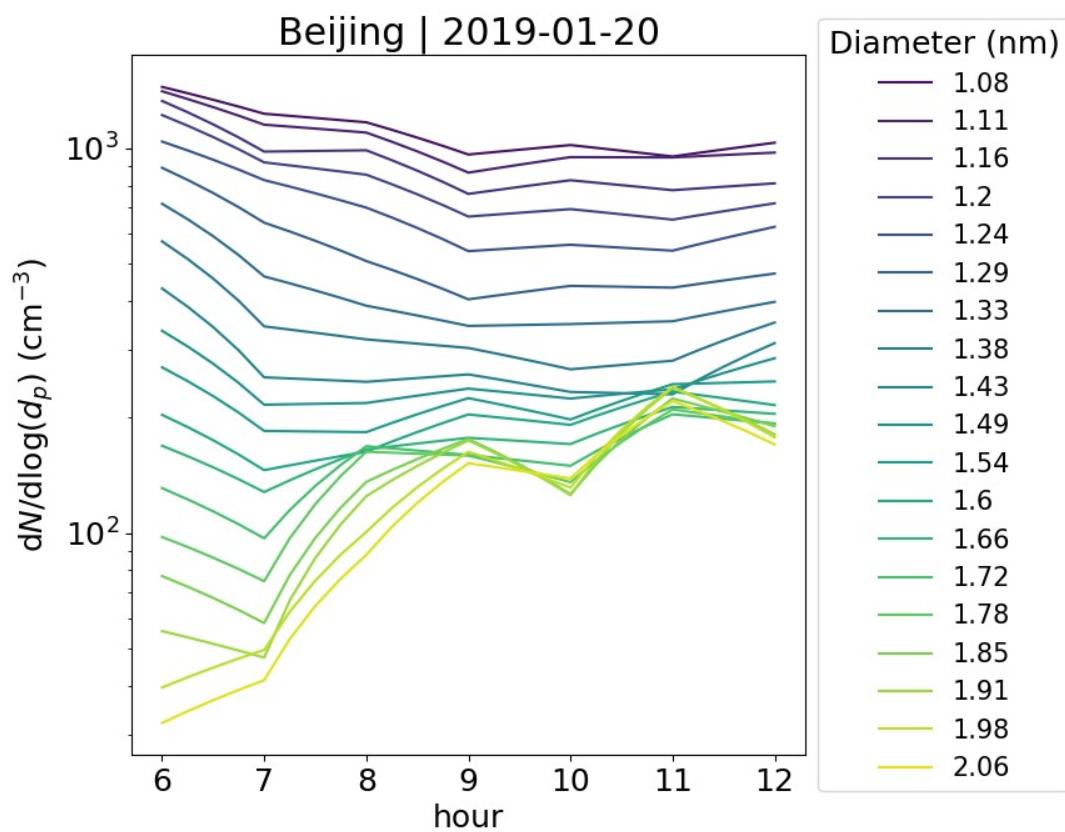
695



696

697 **Fig. A6:** The upper panels show concentrations of ions of a certain diameter with the hour of the
 698 day on 10th of March, 2021 and 19th or April, 2021 in Hyytiälä, Finland. The different colors of the
 699 line indicate the respective ion diameter (d_i). The bottom panels show the appearance time, defined
 700 as the time that the concentration reaches 50% of its maximum, and the respective d_i . The ion
 701 growth rate (GR) derived from these values as a slope of linear regression is shown. For 10th of
 702 March, the GR was determined from 1.24 to 2.05 nm and for 19th of April from 1.43 to 2.05 nm.

703



704

705 **Fig. A7:** The upper panel shows the concentrations of ions of a certain diameter with the hour of the
 706 day on 20th of January, 2019 Beijing, China. The different colors of the line indicate the respective

707 ion diameter (d_i). The bottom panel shows the appearance time, defined as the time that the
708 concentration reaches 50% of its maximum, and the respective d_i . The ion growth rate (GR)
709 derived from these values as a slope of linear regression is shown. The GR was determined from
710 1.72 to 2.06 nm.

711 **References**

- 712 Aalto, P., Hämeri, K., Becker, E., Weber, R., Salm, J., Mäkelä, J. M., Hoell, C., O’ Dowd, C. D.,
713 Hansson, H.-C., Väkevä, M., Koponen, I. K., Buzorius, G., and Kulmala, M.: Physical
714 characterization of aerosol particles during nucleation events, *Tellus B*, 53, 344–358,
715 doi:10.1034/j.1600-0889.2001.530403.x, 2001.
- 716
- 717 Aliaga, D., Tuovinen, S., Zhang, T., Lampilahti, J., Li, X., Ahonen, L., Kokkonen, T., Nieminen, T.,
718 Hakala, S., Paasonen, P., Bianchi, F., Worsnop, D., Kerminen, V.-M., and Kulmala, M.:
719 Nanoparticle ranking analysis: determining new particle formation (NPF) event occurrence and
720 intensity based on the concentration spectrum of formed (sub-5 nm) particles, *Aerosol Research*, 1,
721 81–92, <https://doi.org/10.5194/ar-1-81-2023>, 2023.
- 722
- 723 Arfin, T., Pillai, A.M., Mathew, N., Tirpude, A, Bang, R., and Mondal, P.: An overview of
724 atmospheric aerosol and their effects on human health, *Environ Sci Pollut Res* **30**, 125347–125369,
725 <https://doi.org/10.1007/s11356-023-29652-w>, 2023.
- 726
- 727 Atkinson, R. W., Mills, I. C., Walton, H. A., and Anderson, H. R.: Fine particle components and
728 health—a systematic review and meta-analysis of epidemiological time series studies of daily
729 mortality and hospital admissions. *Journal of exposure science & environmental epidemiology*,
730 25(2), 208–214, <https://doi.org/10.1038/jes.2014.63>, 2015.
- 731
- 732 Bianchi, F., Garmash, O., He, X., Yan, C., Iyer, S., Rosendahl, I., Xu, Z., Rissanen, M. P., Riva, M.,
733 Taipale, R., Sarnela, N., Petäjä, T., Worsnop, D. R., Kulmala, M., Ehn, M., and Junninen, H.: The
734 role of highly oxygenated molecules (HOMs) in determining the composition of ambient ions in the
735 boreal forest, *Atmos. Chem. Phys.*, 17, 13819–13831, <https://doi.org/10.5194/acp-17-13819-2017>,
736 2017.
- 737
- 738 Boucher, O., Randall, D., Artaxo, P., Bretherton, C., Feingold, G., Forster, P., Kerminen, V.-M.,
739 Kondo, Y., Liao, H., Lohmann, U., Rasch, P., Satheesh, S., Sherwood, S., Stevens, B., and Zhan, X.:
740 Clouds and Aerosols, in: *Climate Change 2013: The Physical Science Basis. Contribution of*
741 *Working Group I to the Fifth Assessment Report of the Intergovernmental Panel on Climate*
742 *Change*, edited by: Stocker, T., Qin, D., Plattner, G., Tignor, M., Allen, S., Boschung, J., Nauels, A.,
743 Xia, Y., Bex, V., and Midgley, P., Cambridge University Press, Cambridge, United Kingdom and
744 New York, NY, USA, 571–657, 10, <https://doi.org/10.1017/CBO9781107415324>, 2013.
- 745
- 746 Cai, R., Yan, C., Yang, D., Yin, R., Lu, Y., Deng, C., Fu, Y., Ruan, J., Li, X., Kontkanen, J., Zhang,
747 Q., Kangasluoma, J., Ma, Y., Hao, J., Worsnop, D. R., Bianchi, F., Paasonen, P., Kerminen, V.-M.,
748 Liu, Y., Wang, L., Zheng, J., Kulmala, M., and Jiang, J.: Sulfuric acid–amine nucleation in urban
749 Beijing, *Atmos. Chem. Phys.*, 21, 2457–2468, <https://doi.org/10.5194/acp-21-2457-2021>, 2021.
- 750
- 751
- 752 Dada, L., Paasonen, P., Nieminen, T., Buenrostro Mazon, S., Kontkanen, J., Peräkylä, O., Lehtipalo,
753 K., Hussein, T., Petäjä, T., Kerminen, V.-M., Bäck, J., and Kulmala, M.: Long-term analysis of

754 clear-sky new particle formation events and nonevents in Hyytiälä, *Atmos. Chem. Phys.*, 17, 6227–
755 6241, <https://doi.org/10.5194/acp-17-6227-2017>, 2017.

756

757 Dal Maso, M., Kulmala, M., Riipinen, I., Wagner, R., Hussein, T., Aalto, P. P., and Lehtinen, K. E.
758 J.: Formation and growth of fresh atmospheric aerosols: eight years of aerosol size distribution data
759 from SMEAR II, Hyytiälä, Finland, *Boreal Environ. Res.*, 10, 323–336, 2005.

760

761 Deng, C., Fu, Y., Dada, L., Yan, C., Cai, R., Yang, D., Zhou, Y., Yin, R., Lu, Y., Li, X., Qiao, X.,
762 Fan, X., Nie, W., Kontkanen, J., Kangasluoma, J., Chu, B., Ding, A., Kerminen, V., Paasonen, P.,
763 Worsnop, R. D., Bianchi, F., Liu, Y., Zheng, J., Wang, L., Kulmala, M., and Jiang, J.: Seasonal
764 characteristics of new particle formation and growth in urban Beijing, *Environ. Sci. Technol.*,
765 54, 8547–8557, <https://doi.org/10.1021/acs.est.0c00808>, 2020.

766

767 Ehn, M., Junninen, H., Petäjä, T., Kurtén, T., Kerminen, V.-M., Schobesberger, S., Manninen, H. E.,
768 Ortega, I. K., Vehkamäki, H., Kulmala, M., and Worsnop, D. R.: Composition and temporal behavior
769 of ambient ions in the boreal forest, *Atmos. Chem. Phys.*, 10, 8513–8530, doi:10.5194/acp-10-
770 8513-2010, 2010.

771

772 Ehn, M., Junninen, H., Schobesberger, S., Manninen, H., Franchin, A., Sipilä, M., Petäjä, T.,
773 Kerminen, V.-M., Tammet, H., Mirme, A., Mirme, S., Hõrrak, U., Kulmala, M., and Worsnop, D.
774 R.: An instrumental comparison of mobility and mass measurements of atmospheric small ions,
775 *Aerosol Sci. Tech.*, 45, 522–532, DOI:10.1080/02786826.2010.547890, 2011.

776

777 Fdez-Arroyabe, P., Salcines, C., Kassomenos, P., Santurtún, A., & Petäjä, T.: Electric charge of
778 atmospheric nanoparticles and its potential implications with human health, *Science of the Total*
779 *Environment*, 808, 152106, <https://doi.org/10.1016/j.scitotenv.2021.152106>, 2022.

780

781 Finlay, W. H.: Deposition of aerosols in the lungs: Particle characteristics. *Journal of Aerosol*
782 *Medicine and Pulmonary Drug Delivery*, 34(4), 213–216, doi: 10.1089/jamp.2021.29040.whf,
783 2021.

784

785 Hari, P. and Kulmala, M.: Station for measuring ecosystem-atmosphere relations, *Boreal Environ.*
786 *Res.*, 10, 315–322, 2005.

787

788 Harrison, R. G. and Carslaw, K. S.: Ion-aerosol-cloud processes in the lower atmosphere, *Rev.*
789 *Geophys.*, 41(3), 1012, doi:10.1029/2002RG000114, 2003.

790

791 Harrison, R. G. and Tammet, H.: Ions in Terrestrial Atmosphere and Other Solar System
792 Atmospheres, *Space Sci. Rev.*, 137, 107–118, DOI 10.1007/s11214-008-9356-x, 2008.

793

794 Hirsikko, A., Laakso, L., Hõrrak, U., Aalto, P. P., Kerminen, V.-M. & Kulmala, M.: Annual and
795 size dependent variation of growth rates and ion concentrations in boreal forest. *Boreal Env. Res.*
796 10: 357–369, 2005.

797

798 Hirsikko, A., Bergman, T., Laakso, L., Dal Maso, M., Riipinen, I., Hõrrak, U., and Kulmala, M.:
799 Identification and classification of the formation of intermediate ions measured in boreal forest,
800 *Atmos. Chem. Phys.*, 7, 201–210, <https://doi.org/10.5194/acp-7-201-2007>, 2007.

801

802 Hirsikko, A., Nieminen, T., Gagné, S., Lehtipalo, K., Manninen, H. E., Ehn, M., Hõrrak, U.,
803 Kerminen, V.-M., Laakso, L., McMurry, P. H., Mirme, A., Mirme, S., Petäjä, T., Tammet, H.,

804 Vakkari, V., Vana, M., and Kulmala, M.: Atmospheric ions and nucleation: a review of observations,
805 *Atmos. Chem. Phys.*, 11, 767–798, <https://doi.org/10.5194/acp-11-767-2011>, 2011.

806

807 Hörrak, U., Salm, J., and Tammet, H.: Statistical characterization of
808 air ion mobility spectra at Tahkuse Observatory: Classification of air ions, *J. Geophys. Res.*, 105,
809 9291–9302, 2000.

810

811 Hörrak, U., Aalto, P. P., Salm, J., Komsaare, K., Tammet, H., Mäkelä, J. M., Laakso, L., and
812 Kulmala, M.: Variation and balance of positive air ion concentrations in a boreal forest, *Atmos.*
813 *Chem. Phys.*, 8, 655–675, <https://doi.org/10.5194/acp-8-655-2008>, 2008.

814

815 Jokinen, T., Sipilä, M., Junninen, H., Ehn, M., Lönn, G., Hakala, J., Petäjä, T., Mauldin III, R. L.,
816 Kulmala, M., and Worsnop, D. R.: Atmospheric sulphuric acid and neutral cluster measurements
817 using CI-API-TOF, *Atmos. Chem. Phys.*, 12, 4117–4125, <https://doi.org/10.5194/acp-12-4117-2012>,
818 2012.

819

820 Kirkby, J., Amorim, A., Baltensperger, U., Carslaw, K. S., Christoudias, T., Curtius, J., Donahue, N.
821 M., Haddad, I. E., Flagan, R. C., Gordon, H., Hansel, A., Harder, H., Junninen, H., Kulmala, M.,
822 Kürten, A., Laaksonen, A., Lehtipalo, K., Lelieveld, J., Möhler, O., Riipinen, I., Stratmann, F.,
823 Tomé, A., Virtanen, A., Volkamer, R., Winkler, P. M., and Worsnop, D. R.: Atmospheric new
824 particle formation from the CERN CLOUD experiment, *Nat. Geosci.*, 16, 948–957,
825 <https://doi.org/10.1038/s41561-023-01305-0>, 2023.

826

827 Kulmala, M., Lehtinen, K. E. J., and Laaksonen, A.: Cluster activation theory as an explanation of
828 the linear dependence between formation rate of 3nm particles and sulphuric acid concentration,
829 *Atmos. Chem. Phys.*, 6, 787–793, <https://doi.org/10.5194/acp-6-787-2006>, 2006.

830

831 Kulmala, M., Riipinen, I., Sipilä, M., Manninen, H., Petaja, T., Junninen, H., Dal Maso, M.,
832 Mordas, G., Mirme, A., Vana, M., Hirsikko, A., Laakso, L., Harrison, R., Hanson, I., Leung, C.,
833 Lehtinen, K., and Kerminen, V.: Toward direct measurement of atmospheric nucleation, *Science*,
834 318, 89–92, doi:10.1126/science.1144124, 2007.

835

836 Kulmala, M., Petäjä, T., Nieminen, T., Sipilä, M., Manninen, H. E., Lehtipalo, K., Dal Maso, M.,
837 Aalto, P. P., Junninen, H., Paasonen, P., Riipinen, I., Lehtinen, K. E. J., Laaksonen, A., and
838 Kerminen, V.-M.: Measurement of the nucleation of atmospheric aerosol particles, *Nat. Protoc.*, 7,
839 1651–1667, doi:10.1038/nprot.2012091, 2012.

840

841 Kulmala, M., Kontkanen, J., Junninen, H., Lehtipalo, K., Manninen, H. E., Nieminen, T., Petäjä, T.,
842 Sipilä, M., Schobesberger, S., Rantala, P., Franchin, A., Jokinen, T., Järvinen, E., Äijälä, M.,
843 Kangasluoma, J., Hakala, J., Aalto, P. P., Paasonen, P., Mikkilä, J., Vanhanen, J., Aalto, J., Hakola,
844 H., Makkonen, U., Ruuskanen, T., Mauldin, R. L., Duplissy, J., Vehkamäki, H., Bäck, J.,
845 Kortelainen, A., Riipinen, I., Kurtén, T., Johnston, M. V., Smith, J. N., Ehn, M., Mentel, T. F.,
846 Lehtinen, K. E. J., Laaksonen, A., Kerminen, V.-M., and Worsnop, D. R.: Direct Observations of
847 Atmospheric Aerosol Nucleation, *Science*, 339, 943–946, <https://doi.org/10.1126/science.1227385>,
848 2013.

849

850 Kulmala, M., Kerminen, V. M., Petaja, T., Ding, A. J., and Wang, L.: Atmospheric gas-to-particle
851 conversion: why NPF events are observed in megacities?, *Faraday Discuss.*, 200, 271–288,
852 <https://doi.org/10.1039/c6fd00257a>, 2017.

853

854 Kulmala M., Ezhova E., Kalliokoski T., Noe S., Vesala T., Lohila A., Liski J., Makkonen R., Bäck
855 J., Petäjä T. and Kerminen V.-M.: CarbonSink+ — Accounting for multiple climate feedbacks from
856 forests. *Boreal Env. Res.* 25: 145–159, 2020.

857

858 Kulmala, M., Tuovinen, S., Mirme, S., Koemets, P., Ahonen, L., Liu, Y., Junninen, H., Petäjä, T.,
859 and Kerminen, V.-M.: On the potential of the Cluster Ion Counter (CIC) to observe local new
860 particle formation, condensation sink and growth rate of newly formed particles, *Aerosol Research*,
861 2, 291–301, <https://doi.org/10.5194/ar-2-291-2024>, 2024a.

862

863 Kulmala, M., Ke, P., Lintunen, A., Peräkylä, O., Lohtander, A., Tuovinen, S., Lampilahti, J., Kolari,
864 P., Schiestl-Aalto, P., Kokkonen, T., Nieminen, T., Dada, L., Ylivinkka, I., Petäjä, T., Bäck, J.,
865 Lohila, A., Heimsch, L., Ezhova, E., and Kerminen, V. M.: A novel concept for assessing the
866 potential of different boreal ecosystems to mitigate climate change (CarbonSink+ Potential). *Boreal*
867 *Env. Res.*, 29, 1-16, 2024b.

868

869 Lehtipalo, K., Leppä, J., Kontkanen, J., Kangasluoma, J., Franchin, A., Wimmer, D., Schobesberger,
870 S., Junninen, H., Petäjä, T., Sipilä, M., Mikkilä, J., Vanhanen, J., Worsnop, D. R., and Kulmala, M.:
871 Methods for determining particle size distribution and growth rates between 1 and 3 nm using the
872 Particle Size Magnifier, *Boreal Environ. Res.*, 19, 215–236, 2014.

873

874 Lehtipalo, K., Yan, C., Dada, L., Bianchi, F., Xiao, M., Wagner, R., Stolzenburg, D., Ahonen, L. R.,
875 Amorim, A., Baccarini, A., Bauer, P. S., Baumgartner, B., Bergen, A., Bernhammer, A.-K.,
876 Breitenlechner, M., Brilke, S., Buckholz, A., Mazon, S. B., Chen, D., Chen, X., Dias, A., Dommen,
877 J., Draper, D. C., Duplissy, J., Ehn, M., Finkenzeller, H., Fisher, L., Frege, C., Fuchs, C., Garmash,
878 O., Gordon, H., Hakala, J., He, X. C., Heikkinen, L., Heinrizi, M., Helm, J. C., Hofbauer, V., Hoyle,
879 C. R., Jokinen, T., Kangasluoma, J., Kerminen, V.-M., Kim, C., Kirkby, J., Kontkanen, J., Kürten,
880 A., Lawler, M. J., Mai, H., Mathot, S., Mauldin III, R. L., Molteni, U., Nichman, L., Nie, W.,
881 Nieminen, T., Ojdanic, A., Onnela, A., Passananti, M., Petäjä, T., Piel, F., Pospisilova, V.,
882 Quéléver, L. L. J., Rissanen, M. P., Rose, C., Sarnela, N., Schallhart, S., Sengupta, K., Simon, M.,
883 Tauber, C., Tomé, A., Tröst, J., Väisänen, O., Voge, A. L., Volkamer, R., Wagner, A. C., Wang, M.,
884 Weitz, L., Wimmer, D., Ye, P., Ylisirniö, A., Zha, Q., Carslaw, K., Curtius, J., Donahue, N., Flagan,
885 R. C., Hansel, A., Riipinen, I., Virtanen, A., Winkler, P. M., Baltensperger, U., Kulmala, M., and
886 Worsnop, D. R.: Multi-component new particle formation from sulfuric acid, ammonia and biogenic
887 vapors, *Sci. Adv.*, 4, eaau5363, <https://doi.org/10.1126/sciadv.aau5363>, 2018.

888

889 Li, J., Carlson, B. E., Yung, Y. L., Lv, D., Hansen, J., Penner, J. E., Liao, H., Ramaswamy, V., Kahn,
890 R. A., Zhang, P., Dubovik, O., Ding, A., Lacis, A. A., Zhang, L., and Dong, Y.: Scattering and
891 absorbing aerosols in the climate system, *Nature Reviews Earth & Environment*, 3, 363–379,
892 <https://doi.org/10.1038/s43017-022-00296-7>, 2022.

893

894 Liu, J. Q., Jiang, J. K., Zhang, Q., Deng, J. G., and Hao, J. M.: A spectrometer for measuring
895 particle size distributions in the range of 3 nm to 10 μm, *Front. Env. Sci. Eng.*, 10, 63–72,
896 <https://doi.org/10.1007/s11783-014-0754-x>, 2016.

897

898 Liu, Y., Yan, C., Feng, Z., Zheng, F., Fan, X., Zhang, Y., Li, C., Zhou, Y., Lin, Z., Guo, Y., Zhang,
899 Y., Ma, L., Zhou, W., Liu, Z., Dada, L., Dällenbach, K., Kontkanen, J., Cai, R., Chan, T., Chu, B.,
900 Du, W., Yao, L., Wang, Y., Cai, J., Kangasluoma, J., Kokkonen, T., Kujansuu, J., Rusanen, A., Deng,
901 C., Fu, Y., Yin, R., Li, X., Lu, Y., Liu, Y., Lian, C., Yang, D., Wang, W., Ge, M., Wang, Y., Worsnop,
902 D. R., Junninen, H., He, H., Kerminen, V.-M., Zheng, J., Wang, L., Jiang, J., Petäjä, T., Bianchi, F.,

903 and Kulmala, M.: Continuous and comprehensive atmospheric observations in Beijing: a station to
 904 understand the complex urban atmospheric environment, *Big Earth Data*, 4, 295–321,
 905 <https://doi.org/10.1080/20964471.2020.1798707>, 2020.

906

907 Mazon, S.B., Kontkanen, J., Manninen, H. E., Nieminen, T., Kerminen, V.-M., and Kulmala, M.: A
 908 long-term comparison of nighttime cluster events and daytime ion formation in a boreal forest,
 909 *Boreal Environ. Res.*, 21, 242–261, 2016.

910

911 Mirme, S. and Mirme, A.: The mathematical principles and design of the NAIS – a spectrometer for
 912 the measurement of cluster ion and nanometer aerosol size distributions, *Atmos. Meas. Tech.*, 6,
 913 1061–1071, <https://doi.org/10.5194/amt-6-1061-2013>, 2013.

914

915 Mirme, S., Balbaaki, R., Manninen, H. E., Koemets, P., Sommer, E., Rörup, B., Wu, Y., Almeida, J.,
 916 Ehrhart, S., Weber, S. K., Pfeifer, J., Kangasluoma, J., Kulmala, M., and Kirkby, J.: Design and
 917 performance of the Cluster Ion Counter (CIC), *Atmos. Meas. Tech. Discuss.* [preprint],
 918 <https://doi.org/10.5194/amt-2024-138>, accepted for publication, 2024.

919

920 Quaas, J., Ming, Y., Menon, S., Takemura, T., Wang, M., Penner, J.E., Gettelman, A., Lohmann, U.,
 921 Bellouin, N., Boucher, O., Sayer, A.M., Thomas, G.E., McComiskey, A., Feingold, G., Hoose, C.,
 922 Kristjánsson, J.E., Liu, X., Balkanski, Y., Donner, L. J., Ginoux, P.A., Stier, P., Grandey, B.,
 923 Feichter, J., Sednev, I., Bauer, S.E., Koch, D., Grainger, R.G., Kirkevåg, A., Iversen, T., Seland, Ø.,
 924 Easter, R., Ghan, S.J., Rasch, P.J., Morrison, H., Lamarque, J.-F., Iacono, M. J., Kinne, S., and
 925 Schulz, M.: Aerosol indirect effects – general circulation mode intercomparison and evaluation with
 926 satellite data, *Atmos. Chem. Phys.*, 9, 8697–8717, doi:10.5194/acp-9-8697-2009, 2009.

927

928 Quéléver, L. L. J., Kristensen, K., Normann Jensen, L., Rosati, B., Teiwes, R., Daellenbach, K. R.,
 929 Peräkylä, O., Roldin, P., Bossi, R., Pedersen, H. B., Glasius, M., Bilde, M., and Ehn, M.: Effect of
 930 temperature on the formation of highly oxygenated organic molecules (HOMs) from alpha-pinene
 931 ozonolysis, *Atmos. Chem. Phys.*, 19, 7609–7625, <https://doi.org/10.5194/acp-19-7609-2019>, 2019.

932

933 Rose, C., Zha, Q., Dada, L., Yan, C., Lehtipalo, K., Junninen, H., Mazon, S. B., Jokinen, T., Sarnela,
 934 N., Sipilä, M., Petäjä, T., Kerminen, V.-M., Bianchi, F., and Kulmala, M.: Observations of biogenic
 935 ion-induced cluster formation in the atmosphere, *Sci. Adv.*, 4, 1–11, DOI:[10.1126/sciadv.aar5218](https://doi.org/10.1126/sciadv.aar5218),
 936 2018.

937

938 Zha, Q., Huang, W., Aliaga, D., Peräkylä, O., Heikkinen, L., Koenig, A. M., Wu, C., Enroth, J.,
 939 Gramlich, Y., Cai, J., Carbone, S., Hansel, A., Petäjä, T., Kulmala, M., Worsnop, D., Sinclair, V.,
 940 Krejci, R., Andrade, M., Mohr, C., and Bianchi, F.: Measurement report: Molecular-level
 941 investigation of atmospheric cluster ions at the tropical high-altitude research station Chacaltaya
 942 (5240 m a.s.l.) in the Bolivian Andes, *Atmos. Chem. Phys.*, 23, 4559–4576,
 943 <https://doi.org/10.5194/acp-23-4559-2023>, 2023.

944

945 Schmale, J., Zieger, P., and Ekman, A. M. L.: Aerosols in current and future Arctic climate, *Nat.*
 946 *Clim. Change*, 11, 95–105, <https://doi.org/10.1038/s41558-020-00969-5>, 2021.

947

948 Shiraiwa, M., Ueda, K., Pozzer, A., Lammel, G., Kampf, C. J., Fushimi, A., Enami, S., Arangio, A.
 949 M., Fröhlich-Nowoisky, J., Fujitani, Y., Furuyama, A., Lakey, P. S. J., Lelieveld, J., Lucas, K.,
 950 Morino, Y., Pöschl, U., Takahama, S., Takami, A., Tong, H., Weber, B., Yoshino, A., and Sato, K.:
 951 Aerosol health effects from molecular to global scales, *Environ. Sci. Technol.*, 51, 13545–13567,
 952 <https://doi.org/10.1021/acs.est.7b04417>, 2017.

953

954 Shuman, N. S., Hunton, D. E., and Viggiano, A. A.: Ambient and modified atmospheric ion
955 chemistry: from top to bottom, *Chem. Rev.*, 115, 4542–4570, <https://doi.org/10.1021/cr5003479>,
956 2015.

957

958 Sulo, J., Sarnela, N., Kontkanen, J., Ahonen, L., Paasonen, P., Laurila, T., Jokinen, T.,
959 Kangasluoma, J., Junninen, H., Sipilä, M., Petäjä, T., Kulmala, M., and Lehtipalo, K.: Long-term
960 measurement of sub-3 nm particles and their precursor gases in the boreal forest, *Atmos. Chem.*
961 *Phys.*, 21, 695–715, <https://doi.org/10.5194/acp-21-695-2021>, 2021.

962

963 Tammet, H.: Size and mobility of nanometer particles, clusters and ions, *J. Aerosol Sci.*, 26, 459–
964 475, 1995.

965

966 Tammet, H., Hörrak, U., Laakso, L., and Kulmala, M.: Factors of air ion balance in a coniferous
967 forest according to measurements in Hyytiälä, Finland, *Atmos. Chem. Phys.*, 6, 3377–3390,
968 <https://doi.org/10.5194/acp-6-3377-2006>, 2006.

969

Tammet, H., Komsaare, K., and Horrak, U.: Intermediate ions in the atmosphere, *Atmos. Res.*, 135–
136, 263–273, <https://doi.org/10.1016/j.atmosres.2012.09.009>, 2014.

Tuovinen, S., Lampilahti, J., Kerminen, V.-M., and Kulmala, M.: Intermediate ions as indicator for
local new particle formation, *Aerosol Research*, 2, 93–105, <https://doi.org/10.5194/ar-2-93-2024>,
2024.

Wagner, R., Manninen, H. E., Franchin, A., Lehtipalo, K., Mirme, S., Steiner, G., Petäjä, T., and
Kulmala, M.: On the accuracy of ion measurements using a Neutral cluster and Air Ion
Spectrometer, *Boreal Env. Res.*, 21, 230–241, 2016

Yan, C., Yin, R., Lu, Y., Dada, L., Yang, D., Fu, Y., Kontkanen, J., Deng, C., Garmash, O., Ruan, J.,
Baalbaki, R., Schervish, M., Cai, R., Bloss, M., Chan, T., Chen, T., Chen, Q., Chen, X., Chen, Y.,
Chu, B., Dällenbach, K., Foreback, B., He, X., Heikki-nen, L., Jokinen, T., Junninen, H.,
Kangasluoma, J., Kokkonen, T., Kurppa, M., Lehtipalo, K., Li, H., Li, H., Li, X., Liu, Y., Ma, Q.,
Paasonen, P., Rantala, P., Pileci, R. E., Rusanen, A., Sarnela, N., Simonen, P., Wang, S., Wang, W.,
Wang, Y., Xue, M., Yang, G., Yao, L., Zhou, Y., Kujansuu, J., Petäjä, T., Nie, W., Ma, Y., Ge, M.,
He, H., Donahue, N. M., Worsnop, D. R., Veli-Matti, K., Wang, L., Liu, Y., Zheng, J., Kulmala, M.,
Jiang, J., and Bianchi, F.: The Synergistic Role of Sulfuric Acid, Bases, and Oxidized Organics
Governing New-Particle Formation in Beijing, *Geophys. Res. Lett.*, 48, e2020GL091944,
<https://doi.org/10.1029/2020gl091944>, 2021.

Yao, L., Garmash, O., Bianchi, F., Zheng, J., Yan, C., Kontkanen, J., Junninen, H., Mazon, S. B.,
Ehn, M., Paasonen, P., Sipilä, M., Wang, M., Wang, X., Xiao, S., Chen, H., Lu, Y., Zhang, B., Wang,
D., Fu, Q., Geng, F., Li, L., Wang, H., Qiao, L., Yang, X., Chen, J., Kerminen, V.-M., Petäjä, T.,
Worsnop, D. R., Kulmala, M., and Wang, L.: Atmospheric new particle formation from sulfuric acid
and amines in a Chinese megacity, *Science*, 361, 278–281, <https://doi.org/10.1126/science.aao4839>,
2018.

Yli-Juuti, T., Nieminen, T., Hirsikko, A., Aalto, P. P., Asmi, E., Hörrak, U., Manninen, H. E.,
Patokoski, J., Dal Maso, M., Petäjä, T., Rinne, J., Kulmala, M., and Riipinen, I.: Growth rates of
nucleation mode particles in Hyytiälä during 2003–2009: variation with particle size, season, data
analysis method and ambient conditions, *Atmos. Chem. Phys.*, 11, 12865–12886,
<https://doi.org/10.5194/acp-11-12865-2011>, 2011.

